

1 - 71-4487

(NASA-CR-126914) AERODYNAMIC COEFFICIENTS  
FOR A MODEL OF A PARABOLOIDAL REFLECTOR  
DIRECTIONAL ANTENNA PROPOSED FOR A JPL  
ADVANCED ANTENNA SYSTEM R. B. Blaylock (Jet  
Propulsion Lab.) 1 May 1964 58 p

N72-73008

Unclassified  
00/99 3G910



*Review Copy*

FF No. 602(A)	(ACCESSION NUMBER)	(THRU)
	(PAGES)	(CODE)
	(NASA CR OR TMX OR AD NUMBER)	(CATEGORY)
	AVAILABLE TO NASA OFFICES AND NASA RESEARCH CENTERS ONLY	

JET PROPULSION LABORATORY  
CALIFORNIA INSTITUTE OF TECHNOLOGY  
PASADENA, CALIFORNIA

RE-ORDER NO. 64-213

Internal Memorandum CP-6

AERODYNAMIC COEFFICIENTS FOR A MODEL  
OF A PARABOLOIDAL-REFLECTOR DIREC-  
TIONAL ANTENNA PROPOSED FOR A  
JPL ADVANCED ANTENNA SYSTEM

Robert B. Blaylock

Bain Dayman, Jr.

Bain Dayman, Jr., Chief  
Aerodynamic Facilities Section

JET PROPULSION LABORATORY  
CALIFORNIA INSTITUTE OF TECHNOLOGY  
PASADENA, CALIFORNIA  
May 1, 1964

115 58 PAGES

RE-ORDER No. 64-213

Copyright © 1964  
Jet Propulsion Laboratory  
California Institute of Technology

Prepared Under Contract No. NAS 7-100  
National Aeronautics & Space Administration

## CONTENTS

I.	Introduction . . . . .	1
II.	Test Description . . . . .	2
	A. Wind Tunnel and Instrumentation . . . . .	2
	B. Wind-Tunnel Model . . . . .	2
	C. Data and Data Reduction . . . . .	4
III.	Discussion of Results . . . . .	5
	A. Forces and Moments of the Basic Configuration . . . . .	5
	B. Contribution of the Alidade on the Forces and Moments . . . . .	5
	C. Effect of Changes in the Reflector Support Structure on Forces and Moments . . . . .	5
	D. Effect of Changes in the Base on Forces and Moments . . . . .	6
	E. Effect of Boundary-Layer Velocity Profile on Forces and Moments . . . . .	6
	F. Axial Loads on the Legs of the Quadripod Support for the Cassegrain Reflector . . . . .	6
IV.	Summary . . . . .	7
	References . . . . .	8
	Table I. Coefficient Repeatability . . . . .	9

## FIGURES

1.	Boundary-layer generator in place . . . . .	10
2.	Velocity profiles related to antenna . . . . .	11
3.	Basic configuration alidade metric, side view . . . . .	12
4.	Basic configuration alidade metric, rear three-quarter view . . . . .	13
5.	Basic configuration with no porosity in reflector . . . . .	14
6.	Basic configuration with additional reflector support structure . . . . .	15
7.	Basic configuration with reflector support structure closed . . . . .	16
8.	Basic configuration with reflector support structure partially closed . . . . .	17
9.	Basic configuration with reflector support structure partially closed-edge open . . . . .	18
10.	Basic configuration with alidade removed . . . . .	19
11.	Basic configuration alidade nonmetric . . . . .	20

## FIGURES (Cont'd)

12. Basic configuration with cone base . . . . .	21
13. Basic configuration with wind up-flow shield on cylinder base . . . . .	22
14. Quadripod structure leg-code numbers . . . . .	23
15. Stability-axis system . . . . .	24
16. Basic configuration with control rooms and elevator removed . . . . .	25
17. Effect of antenna attitude on lift-force coefficient . . . . .	26
18. Effect of antenna attitude on axial-force coefficient . . . . .	27
19. Effect of antenna attitude on lateral-force coefficient . . . . .	28
20. Effect of antenna attitude on yaw-moment coefficient . . . . .	29
21. Effect of antenna attitude on pitch-moment coefficient . . . . .	30
22. Effect of antenna attitude on roll-moment coefficient . . . . .	31
23. Contributions of alidade on lift-force coefficient . . . . .	32
24. Contributions of alidade on axial-force coefficient . . . . .	33
25. Contributions of alidade on lateral-force coefficient . . . . .	34
26. Contributions of alidade on yaw-moment coefficient . . . . .	35
27. Contributions of alidade on pitch-moment coefficient . . . . .	36
28. Contributions of alidade on roll-moment coefficient . . . . .	37
29. Effect of changes in the reflector support structure on lift-force coefficient . . . . .	38
30. Effect of changes in the reflector support structure on axial-force coefficient . . . . .	39
31. Effect of changes in the reflector support structure on lateral-force coefficient . . . . .	40
32. Effect of changes in the reflector support structure on yaw-moment coefficient . . . . .	41
33. Effect of changes in the reflector support structure on pitch-moment coefficient . . . . .	42
34. Effect of changes in the reflector support structure on roll-moment coefficient . . . . .	43
35. Effect of velocity gradients on lift-force coefficient . . . . .	44
36. Effect of velocity gradients on axial-force coefficient . . . . .	45
37. Effect of velocity gradients on lateral-force coefficient . . . . .	46
38. Effect of velocity gradients on yaw-moment coefficient . . . . .	47

## FIGURES (Cont'd)

- |  |    |
|--|----|
| 39. Effect of velocity gradients on pitch-moment coefficient . . . . . | 48 |
| 40. Effect of velocity gradients on roll-moment coefficient . . . . .  | 49 |
| 41. Axial-force coefficient on leg 1 of quadripod structure . . . . .  | 50 |
| 42. Axial-force coefficient on leg 2 of quadripod structure . . . . .  | 51 |
| 43. Axial-force coefficient on leg 3 of quadripod structure . . . . .  | 52 |
| 44. Axial-force coefficient on leg 4 of quadripod structure . . . . .  | 53 |

## ABSTRACT

This Report presents force- and moment-coefficients for wind loads on a model of a proposed, large, paraboloidal-reflector antenna. The wind-tunnel model has a reflector diameter of 18 in., which gives a scale factor of 1 to 140. The data are taken at a nominal dynamic pressure of 150 lb/ft<sup>2</sup>, giving a Reynolds No. of  $3.4 \times 10^6$  based on reflector diameter. Several modifications to the basic configuration are made to check the effect of possible design changes, such as reflector porosity, depth of reflector support structure, shielding of reflector porosity, and base design. A discussion of data interpretation for different vertical wind-velocity profiles is included. Also presented are coefficients for axial loads on the legs of the quadripod support structure, inside the reflector, for the cassegrain reflector.

## I. INTRODUCTION

Large antennas of the type used in tracking orbital and interplanetary flight are sensitive to wind loads (Ref. 1). These antennas must be able to maintain reflector surface shape and to track during critical phases of the trajectory, regardless of wind conditions. A number of large antennas is in existence, but the amount of wind-load data for design purposes is limited.

This Report presents data for a relatively detailed model of a paraboloidal-reflector directional antenna being considered for use in the advanced antenna system by the Deep-Space Instrumentation Facility (DSIF) of the Jet Propulsion Laboratory (JPL). A previous test (Ref. 2 and 3) was run on simplified paraboloidal-antenna models to secure basic force, moment, and pressure data.

## II. TEST DESCRIPTION

A. Wind Tunnel and Instrumentation

This test was conducted in July, 1962 at the Northrop (Hawthorne, Calif.) subsonic wind tunnel under the supervision of Mr. Norman L. Fox. The wind tunnel has a test section that is 7 ft x 10 ft in cross section and is 20 ft long. The data were taken at a nominal dynamic pressure of 150 lb/ft<sup>2</sup>, giving a Reynolds No. of  $3.4 \times 10^6$  based on reflector diameter. A few runs were made at a nominal dynamic pressure of 50 lb/ft<sup>2</sup> for a Reynolds-number check ( $2 \times 10^6$ ) and to secure data on the quadripod structure of the cassegrain reflector.

The normal boundary layer in the tunnel was 3.61 in. thick. The boundary-layer thickness was considered as the distance between the tunnel floor and the point where the local wind velocity was 99% of the free-stream velocity. With a 15-in.-high "picket-fence-type" boundary-layer generator spanning the test-section floor at the entrance (Fig. 1), the boundary-layer thickness was increased to 17.87 in. While this increase was not expected to duplicate an on-site wind profile, it did give a reasonably smooth profile gradient (Fig. 2). The profile gradients were measured during the first test (Ref. 2 and 3). The relative position of the antenna reflector to the velocity profile is shown as the antenna moved through the elevation-angle travel (Fig. 2). Data taken with the boundary-layer generator in use were run with a nominal dynamic pressure of 100 lb/ft<sup>2</sup> (Table 1).

The wind-tunnel balance and read-out equipment were calibrated relative to the position of the model in the tunnel.

B. Wind-Tunnel Model

The basic model configuration is shown in Fig. 3 and 4. The model paraboloidal reflector was spin-formed of commercial copper sheet which was 1/8 in. thick and had a diameter of 18 in. The model had a focal distance to diameter ratio of 0.420, or depth to reflector diameter ratio of 0.1488. Holes of 3/16 in. diameter were drilled in a uniform pattern on the outer 25% of the reflector radius to obtain 25% porosity of that area. Pressure-sensitive tape was used to vary the porosity (Fig. 5).

Several changes were made to the simulated-reflector support structure. The basic reflector support structure was 1 and 13/16 in. deep at the point of maximum thickness. Figure 6 shows the model with an additional structure on back of the basic reflector support structure (the addition is shown in place and also removed). The addition was 1 in. deep at the corresponding maximum thickness point in order to give an over-all thickness of 2 and 13/16 in. The reflector support structure was also completely closed with no porosity in the reflector, as in Fig. 7. A partially closed (2 and 1/4 in. wide) support structure with porosity in the reflector is shown in Fig. 8 and 9.

The alidade structure was 7 and 3/8 in. high. The alidade was considered as that part of the model structure between the azimuth and elevation bearings. Figure 10 shows the antenna with the alidade removed, showing azimuth and elevation bearings. Figures 3 and 4 show the alidade in position and attached at the elevation bearing. Figure 11 shows the alidade in position and attached at the azimuth bearing. Two base designs were used, viz., (1) a cylinder, 2 and 1/8 in. high with an 8-in. diameter (Fig. 3), and (2) the frustum of a cone, 2 and 1/4 in. high with an 8 and 1/16-in. diameter at the top and a 10 and 9/16-in. diameter at the bottom (Fig. 12). A wind up-flow shield, 1 and 3/16 in. wide, was attached to the top of the cylinder base (Fig. 13). The reflector was supported from the external balance on a 1 and 5/8-in. staff which incorporated integral pitch and roll gages. A serrated joint in the top of the staff allowed elevation changes from 0 to 180 deg in 5-deg increments. Azimuth angle changes from -15 to 195 deg were made by rotation of the balance by remote control. All of the structure of the model was mounted to the copper paraboloidal reflector, with the exception of the base and the alidade when the alidade was nonmetric.

The coincident intersection, of (1) the azimuth and elevation axes of rotation and (2) the paraboloidal centerline, was placed 9 and 5/8 in. above the tunnel floor.

The quadripod legs were machined from 0.250 by 0.375-in. rectangular tubing in order to represent structural columns. These four legs, each 9.88 in. long and rigidly connected at their apex, were attached to the paraboloidal reflector by means of load cells arranged to read this axial load in each leg individually. The hyperbolic cassegrain reflector had a 1.72-in. diameter. In Fig. 14, a reference code is pictured for use with the data for each leg.

**C. Data and Data Reduction**

All data were reduced on a digital computer and plotted by automatic equipment. The data presented in this Report were selected from these working plots. Corrections of dynamic pressure were made for tunnel test-section blockage due to the model. These corrections were based on private correspondence with Mr. R. W. F. Gould, Aerodynamics Division, National Physical Laboratory, Teddington, Middlesex, England.

All data presented in this Report were in the stability axis-system orientation shown in Fig. 15 and described in Ref. 2, with the moment center at the intersection of the azimuth and elevation axes of rotation. This center was on the paraboloidal axis of symmetry, 0.1423 reflector diameters aft of the vertex. Conventional aerodynamic terminology was used in this Report.

The force- and moment-coefficients presented in this Report were in the form of the customary nondimensional aerodynamic coefficients. The force-coefficients were defined as follows:

$$\frac{\text{force}}{(\text{dynamic pressure})(\text{reflector frontal area})}$$

The moment-coefficients were defined as follows:

$$\frac{\text{moment}}{(\text{dynamic pressure})(\text{reflector frontal area})(\text{reflector diameter})}$$

The dynamic pressure was defined as follows:

$$1/2 (\text{ambient static air density})(\text{air velocity})^2$$

The most complete set of data was obtained on the basic configuration, and tests of the other configurations were made in areas where differences might be significant. Comparison data were obtained by removing and adding components to the basic configuration. These configuration changes consisted of changes in the reflector porosity (Fig. 5), different base designs (Fig. 3, 12, and 13), addition and subtraction of the cassegrain reflector, control houses, and elevator (Fig. 16), and variations of the reflector support structure (Fig. 6, 7, 8, and 9). Data were not taken at the 0-deg elevation angle but were taken at a

5-deg elevation angle, due to interference, in most cases, of the reflector support structure and the staff. Basic data were taken with all structure above the base metric. The term metric indicated that the structure was connected to the balance, in order that the load due to the wind might be recorded. The term nonmetric indicated that the structure was not connected to the balance, although in position.

Comparison data were taken with the alidade (1) nonmetric (Fig. 12) and (2) absent (Fig. 11).

### III. DISCUSSION OF RESULTS

#### A. Forces and Moments of the Basic Configuration

Figures 17 through 22 present the force- and moment-coefficients of the basic configuration shown in Fig. 3 and 4. The force- and moment-coefficients were plotted against antenna attitude. All of the forces and moments were acting at the intersection of the azimuth and elevation axes of rotation. The wind load was measured on all structure above the base (above the plane of the azimuth bearing).

The axial force, lateral force, and yaw-moment coefficients showed a peak load at elevation angle of 5 deg (limit of data), while lift-force coefficient and pitch-moment coefficient peaks occurred at the 50 to 60-deg elevation angle; roll-moment coefficient peak occurred at the 75-deg elevation angle.

#### B. Contribution of the Alidade on the Forces and Moments

A set of comparison plots, Fig. 23 through 28, shows the contribution of the alidade to the force- and moment-coefficients. The data for the alidade nonmetric were shown in conjunction with the data for the alidade metric. The difference between corresponding points on the curves was the contribution of the alidade. The alidade showed small effects on lift force, drag force, pitch moment, and yaw moment. The lateral force and roll moment increased significantly as the antenna approached 90-deg azimuth or elevation angle.

#### C Effect of Changes in the Reflector Support Structure on Forces and Moments

Several changes in the reflector support structure were made, and significant changes in peak loads were found in some cases. One purpose of this

series of structural changes was to try to optimize the antenna to a solid reflector for low-noise leakage and to have a porous rim for aerodynamic properties found to be desirable in Ref. 2. These comparisons are shown in Fig. 29 through 34.

With additional structure, there were no changes in force- and moment-coefficient within the accuracy of the data. With the complete reflector support structure closed and no porosity on the reflector, the force- and moment-coefficients compared closely to the basic structure with no porosity on the reflector; the exception was related to pitch and roll-moment coefficients in the peak coefficient range of 50 to 75-deg azimuth angle.

A possible compromise is pictured in Fig. 8 and 9, where a partially closed support structure was used. The reflector was left as rim-porous with a shield placed directly behind the porous section. This shield, while giving a blocking effect to noise, allowed air passage through the reflector edge. This air passage kept the force- and moment-coefficients comparable to the basic configuration coefficients. The configuration in Fig. 9 (partially closed reflector support structure with the edge left open) may give the best compromise from reflection and aerodynamic viewpoints.

#### D. Effect of Changes in the Base on Forces and Moments

No measurable effect was found in forces or moments with changes in base configurations.

#### E. Effect of Boundary-Layer Velocity Profile on Forces and Moments

The force- and moment-coefficients presented in Fig. 35 through 40 have been made nondimensional, using the dynamic pressure at the force- and moment-center. The local dynamic pressure at the force- and moment-center had a ratio of 0.79 to the free-stream dynamic pressure. From the correlation shown, it seemed that this would be a reasonable method to use on an on-site velocity gradient.

#### F. Axial Loads on the Legs of the Quadripod Support for the Cassegrain Reflector

Figures 41 through 44 present the axial-force coefficients for the quadripod legs. Due to redundancy in the mounting and model-testing problems, these data had an estimated accuracy of  $\pm 0.001$  in coefficient. Within this accuracy,

basic antenna configuration changes (such as paraboloidal-reflector surface, rim-porous, vs all solid supporting-structure changes), and even the presence or absence of the hyperbolic cassegrain reflector, had little effect.

#### IV. SUMMARY

Presented in this Report are the force- and moment-coefficients due to wind loads on a paraboloidal-reflector antenna model. Several modifications to the basic design were made to secure data for possible design changes.

## REFERENCES

1. Jet Propulsion Laboratory, California Institute of Technology. Project Description: Advanced Antenna System for the Deep-Space Instrumentation Facility. Pasadena, Calif., JPL, October 12, 1960. (EPD No. 5, Rev. 1) UNCLASSIFIED
2. Jet Propulsion Laboratory, California Institute of Technology. Preliminary Report on Paraboloidal-Reflector-Antenna Wind-Tunnel Tests, by N. L. Fox and B. Dayman, Jr. Pasadena, Calif., JPL, February 28, 1962. (JPL IM CP-3) UNCLASSIFIED
3. Jet Propulsion Laboratory, California Institute of Technology. Load Distributions on the Surface of Paraboloidal-Reflector Antennas, by N. L. Fox. Pasadena, Calif., JPL, July, 1962. (JPL IM CP-4) UNCLASSIFIED

## INTERNAL MEMORANDUM

Table 1. Coefficient repeatability

Coefficient*	Dynamic Pressure (150 lb/ft <sup>2</sup> )	Dynamic Pressure (100 lb/ft <sup>2</sup> )
Lift-force coefficient	0.002	0.002
Axial-force coefficient	0.010	0.007
Lateral-force coefficient	0.004	0.003
Yaw-moment coefficient	0.0018	0.0012
Pitch-moment coefficient	0.0026	0.0018
Roll-moment coefficient	0.0038	0.0025

\* Based on a reflector frontal area of 101.7875 in.<sup>2</sup> and a reflector diameter of 18 in.

RE-ORDER No. 64-213

INTERNAL MEMORANDUM

JPL CP-6

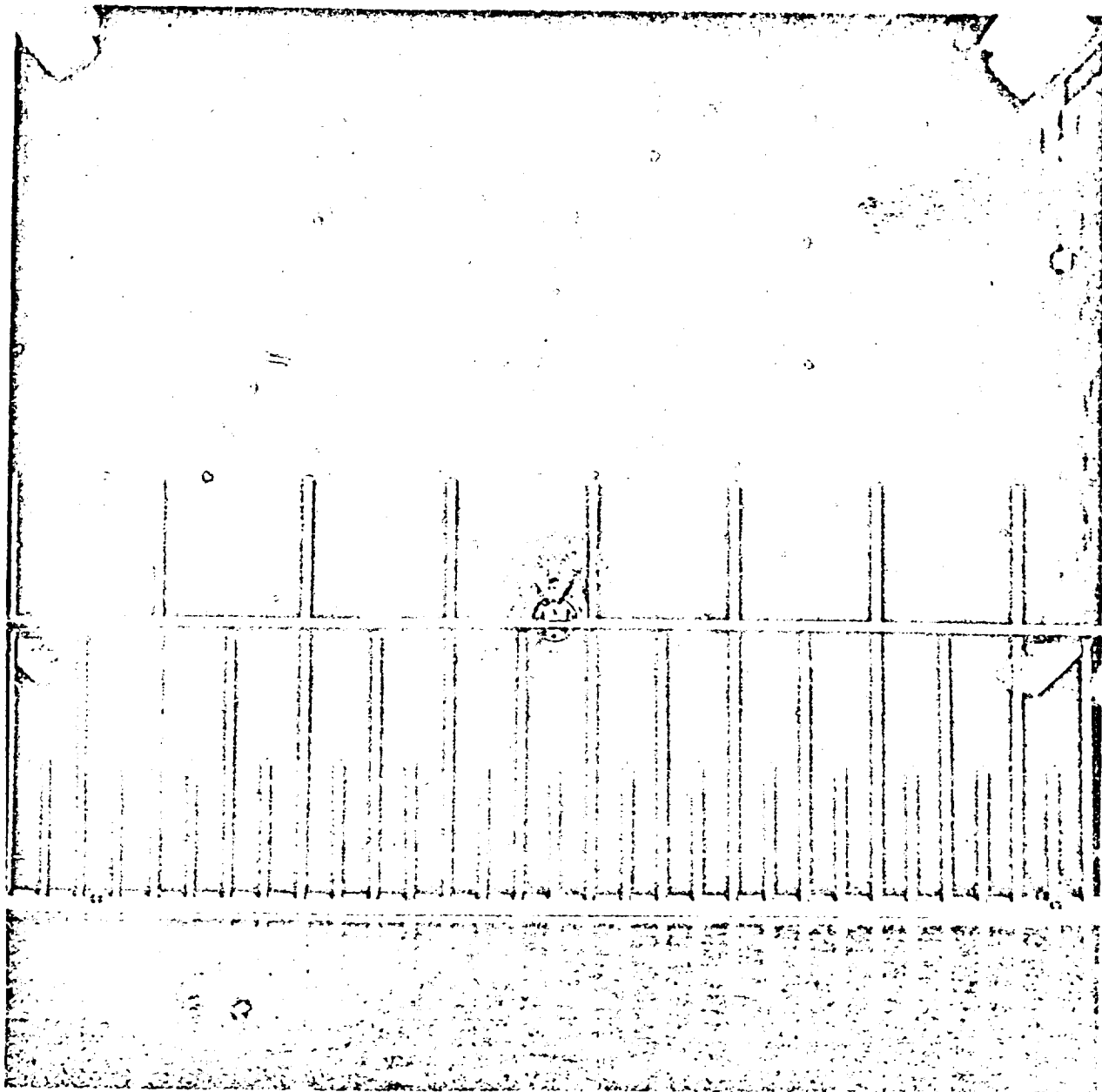


Fig. 1. Boundary-layer generator in place

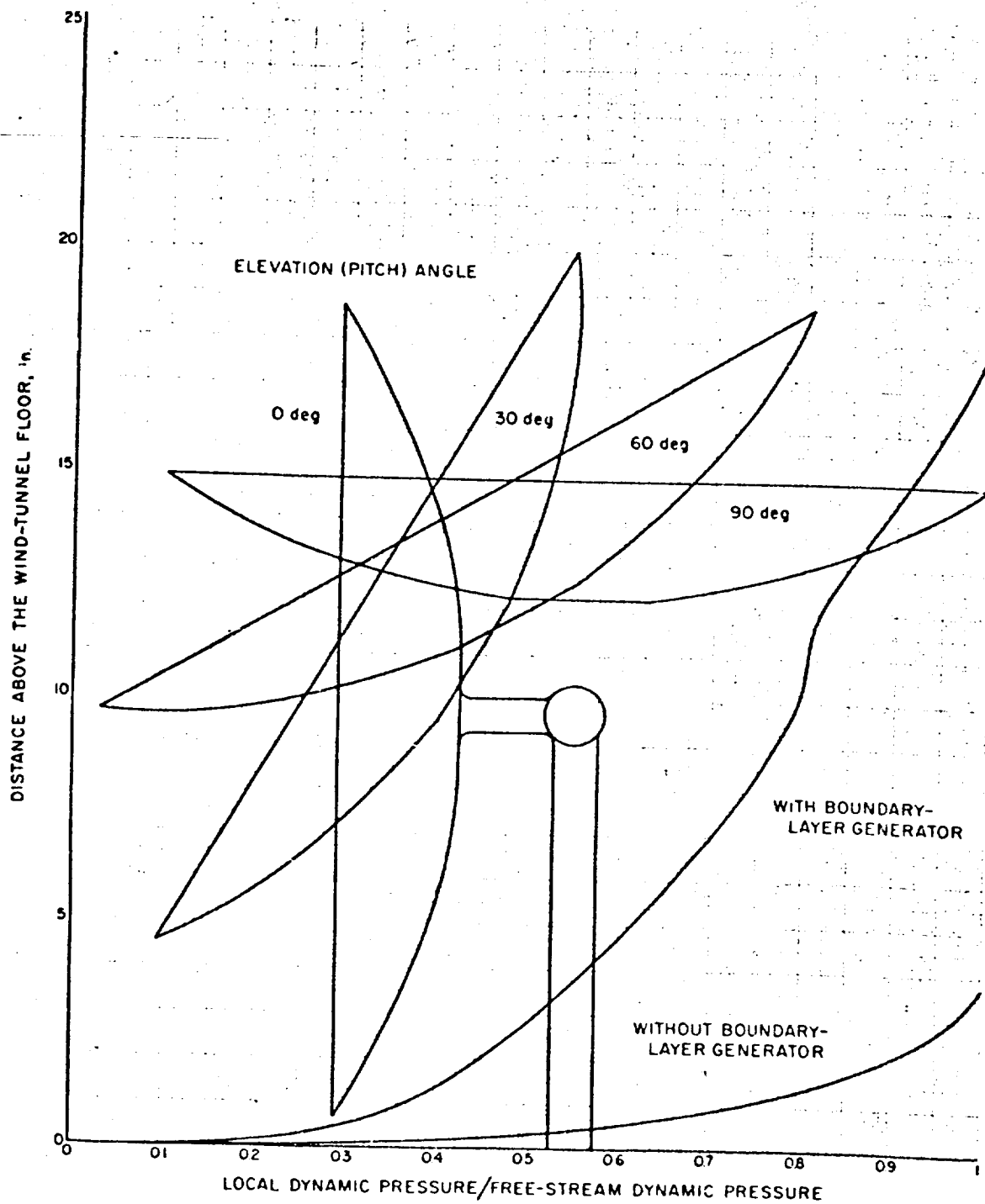


Fig. 2. Velocity profiles related to antenna

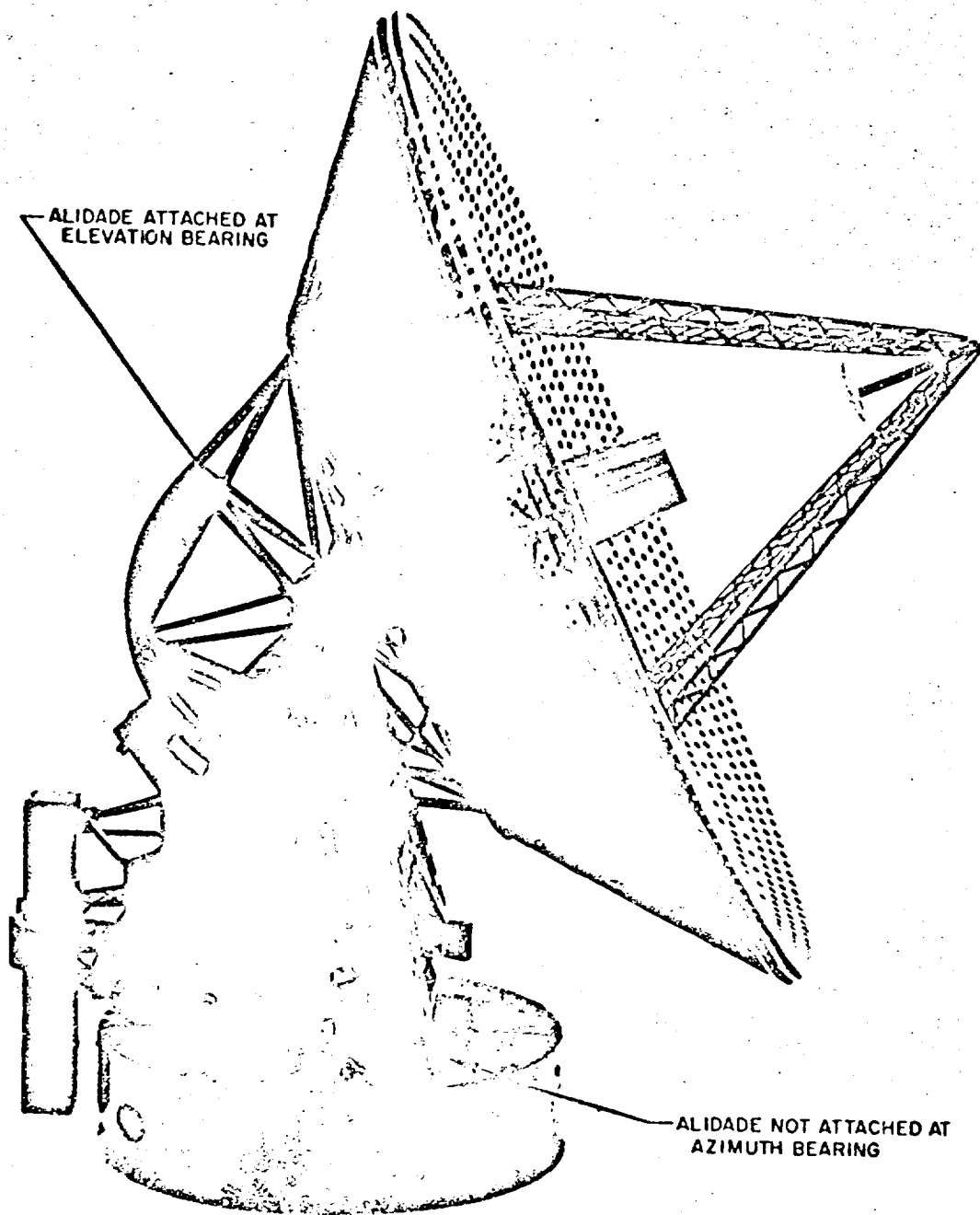


Fig. 3. Basic configuration alidade metric, side view

RE-ORDER No. 64-213

INTERNAL MEMORANDUM

JPL CP-6

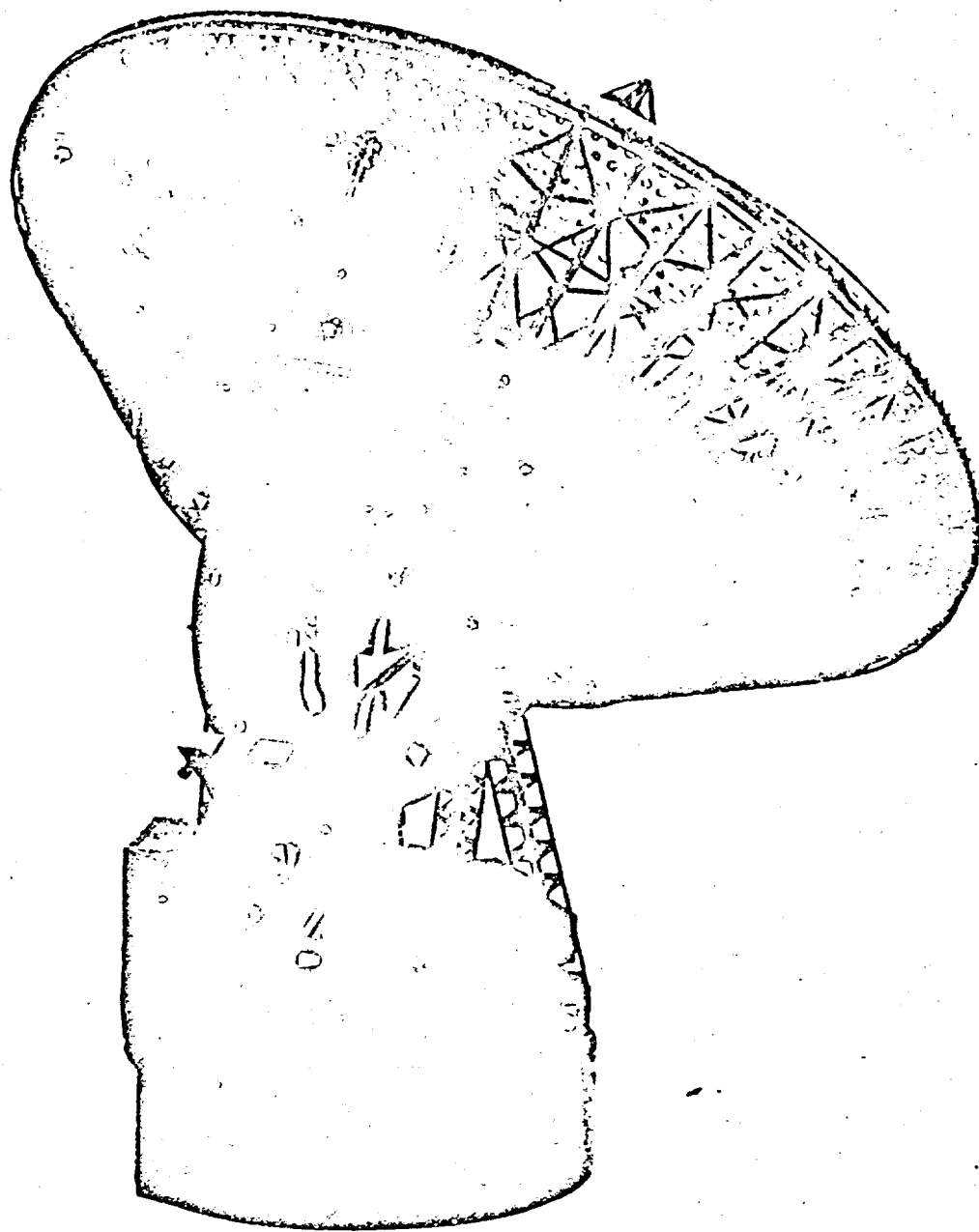


Fig. 4. Basic configuration alidade metric, rear three-quarter view

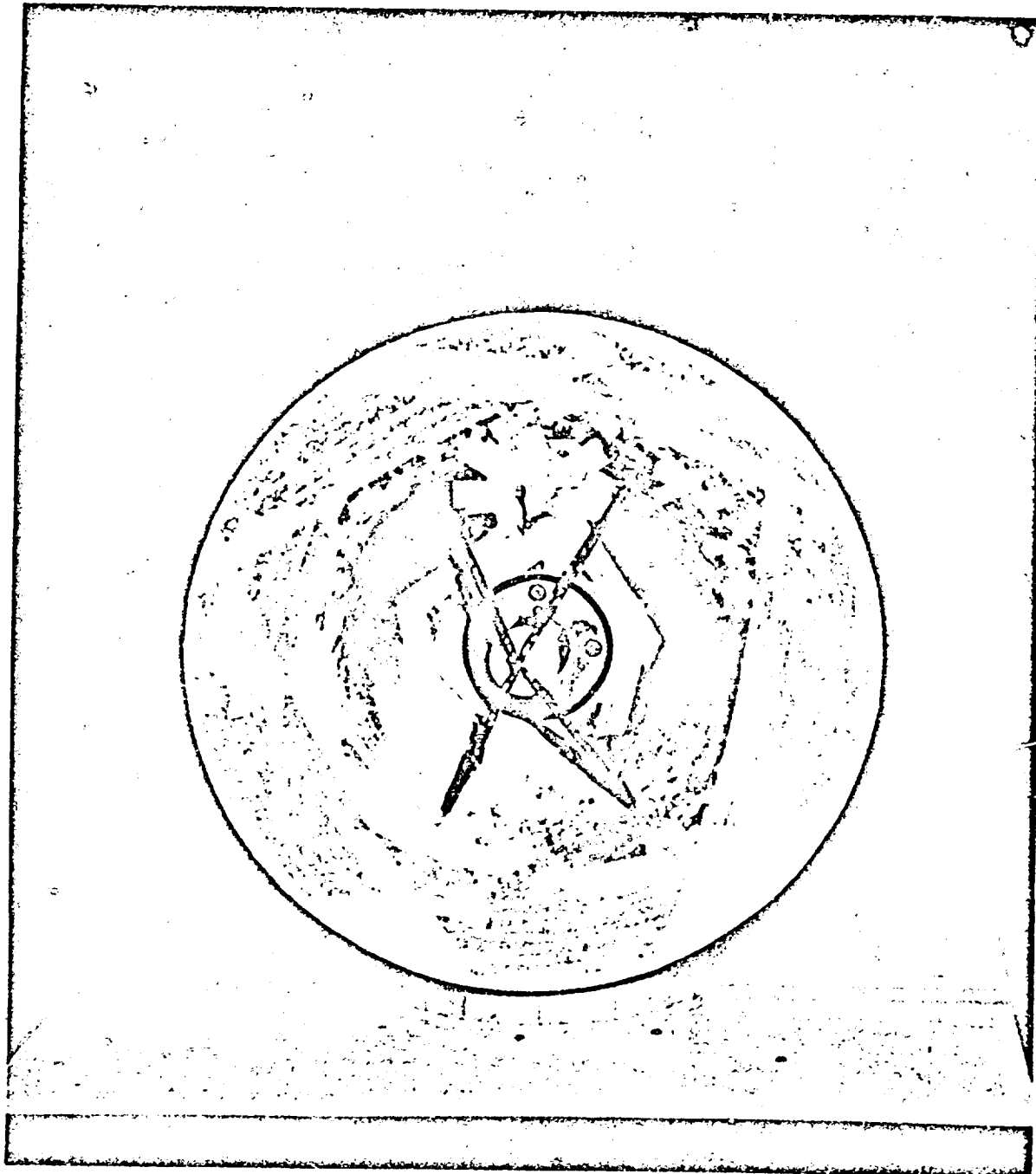


Fig. 5. Basic configuration with no porosity in reflector

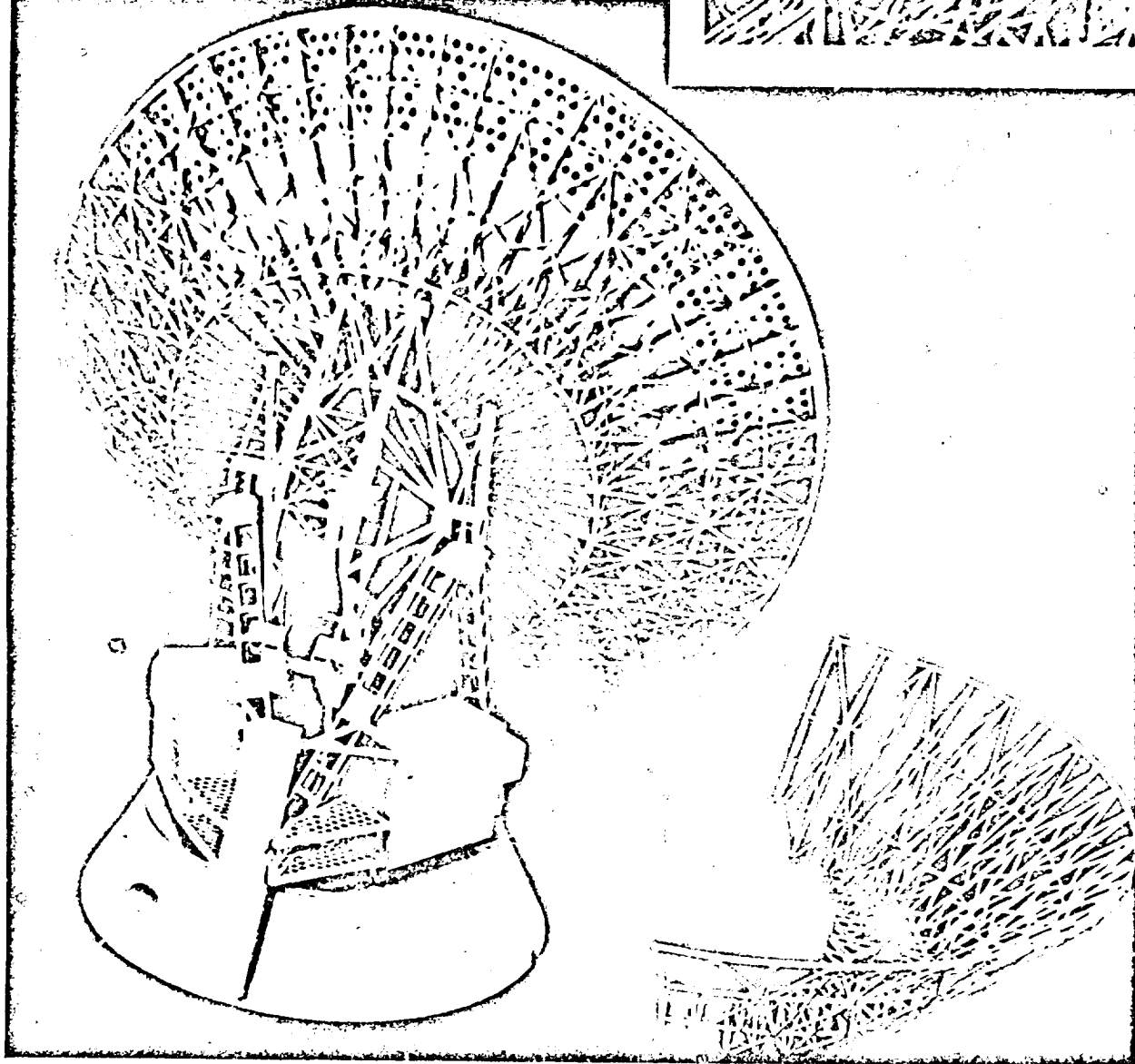


Fig. 6. Basic configuration with additional reflector support structure

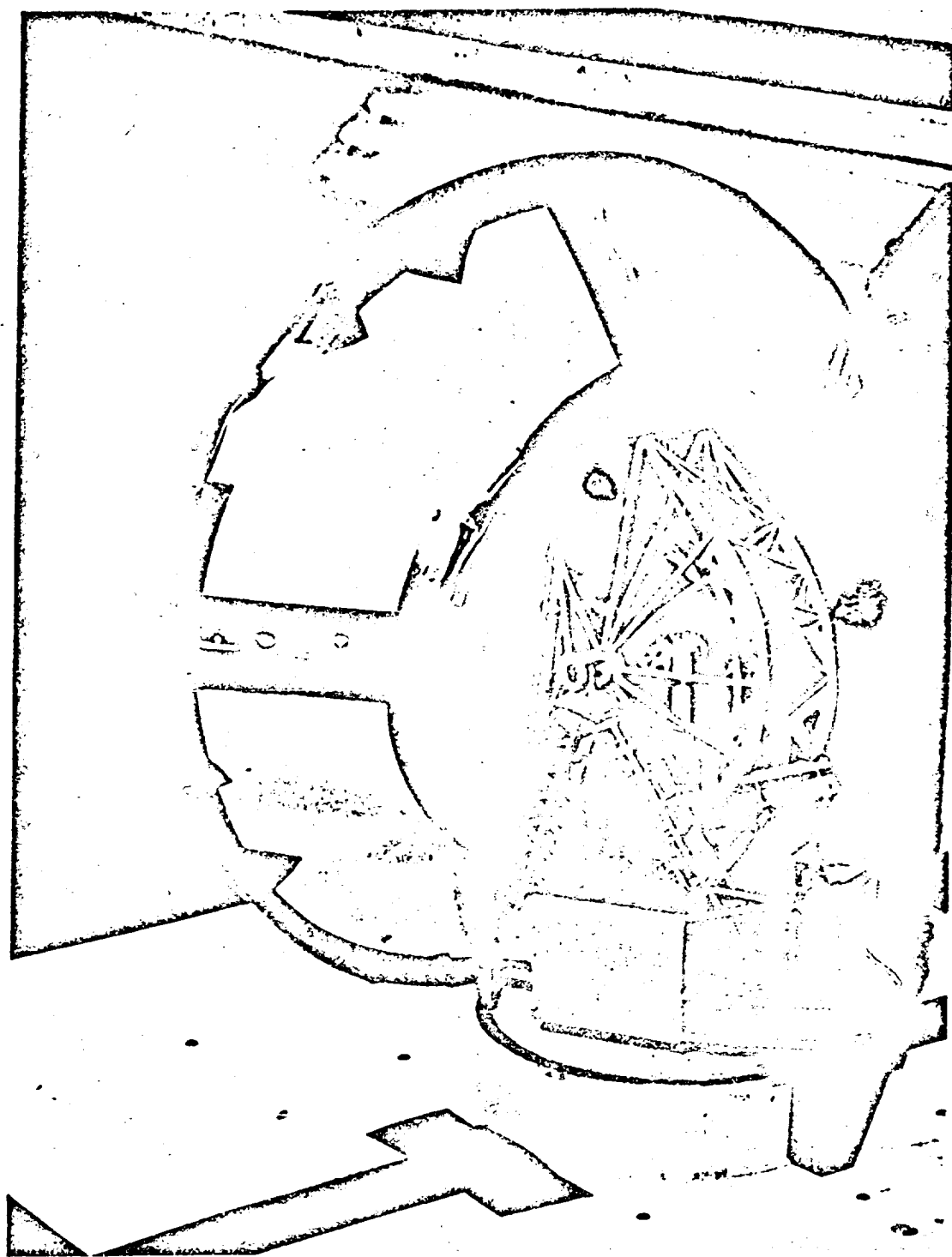


Fig. 7. Basic configuration with reflector support structure closed

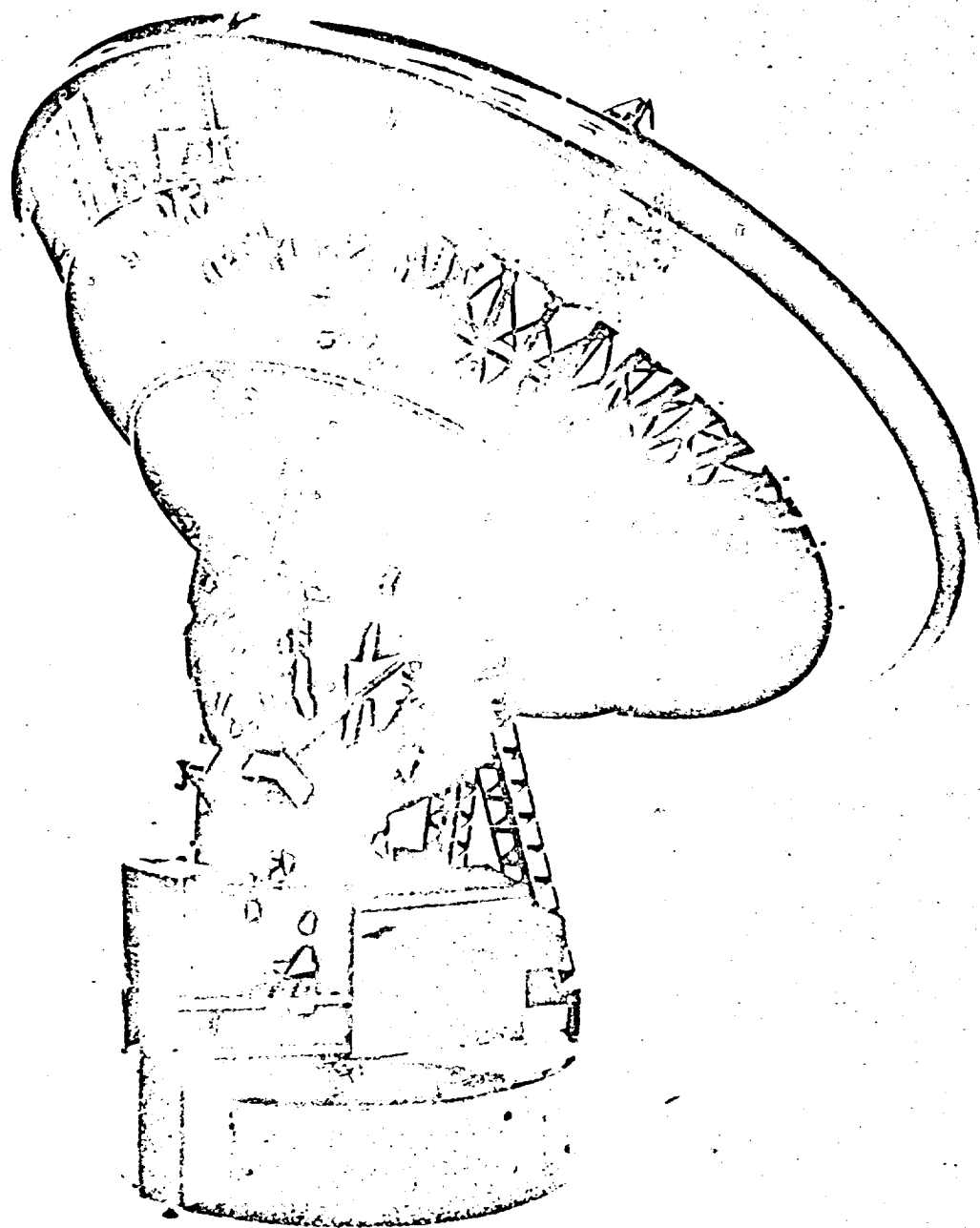


Fig. 8. Basic configuration with reflector support structure partially closed

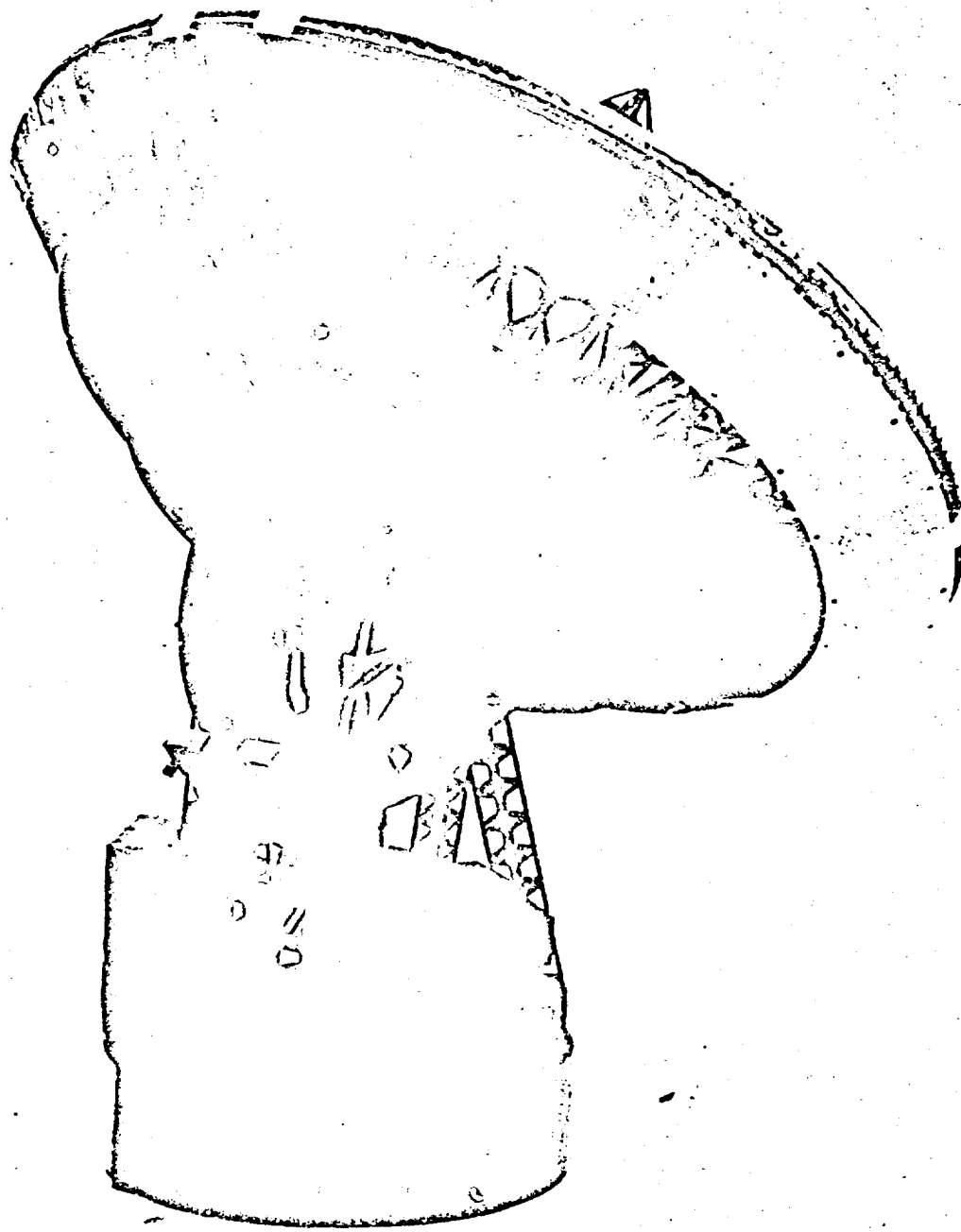


Fig. 9. Basic configuration with reflector support structure partially closed-edge open

REORDER No. 64-213

INTERNAL MEMORANDUM

JPL CP-6

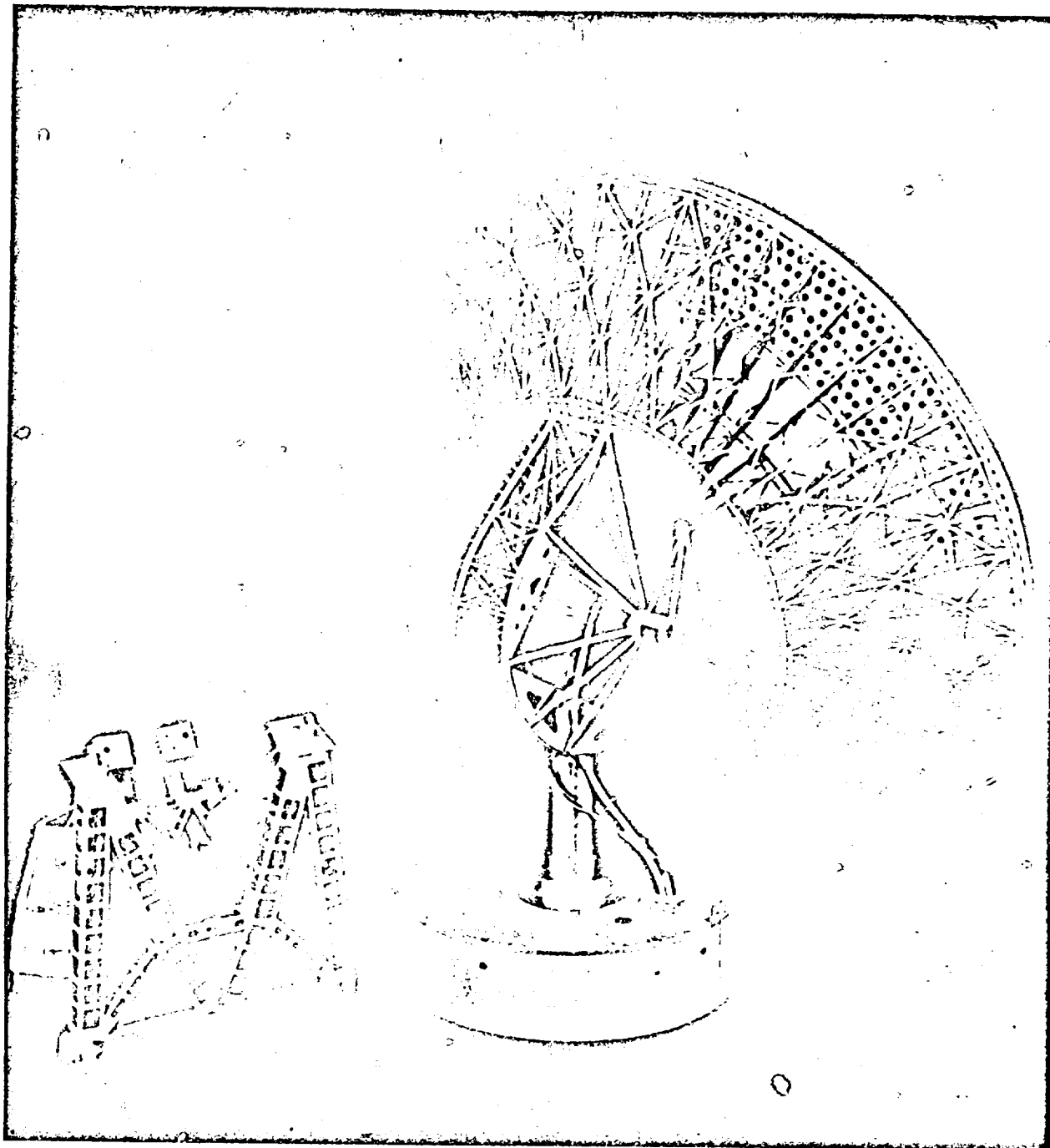


Fig. 10. Basic configuration with alidade removed

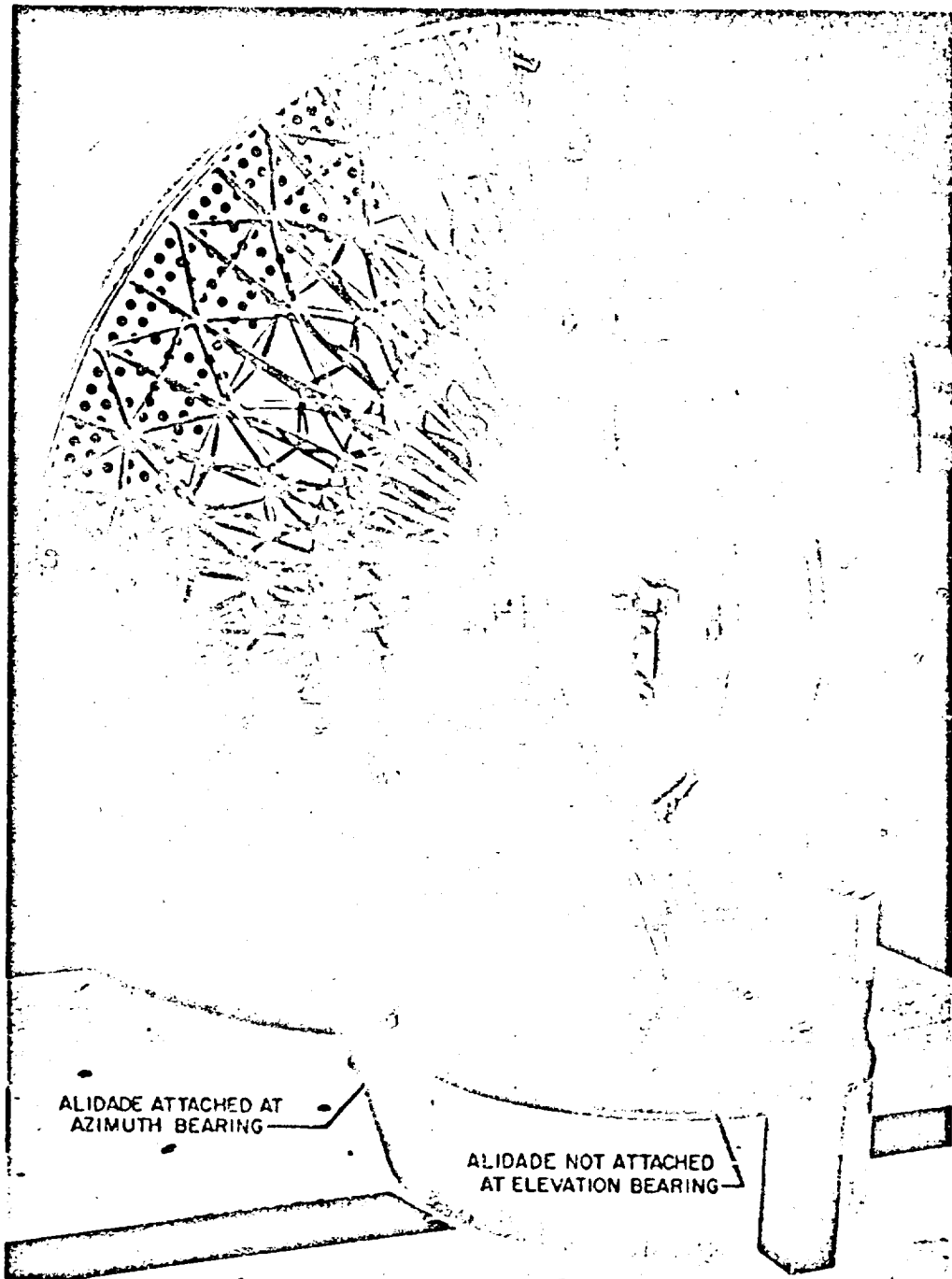


Fig. 11. Basic configuration alidade nonmetric

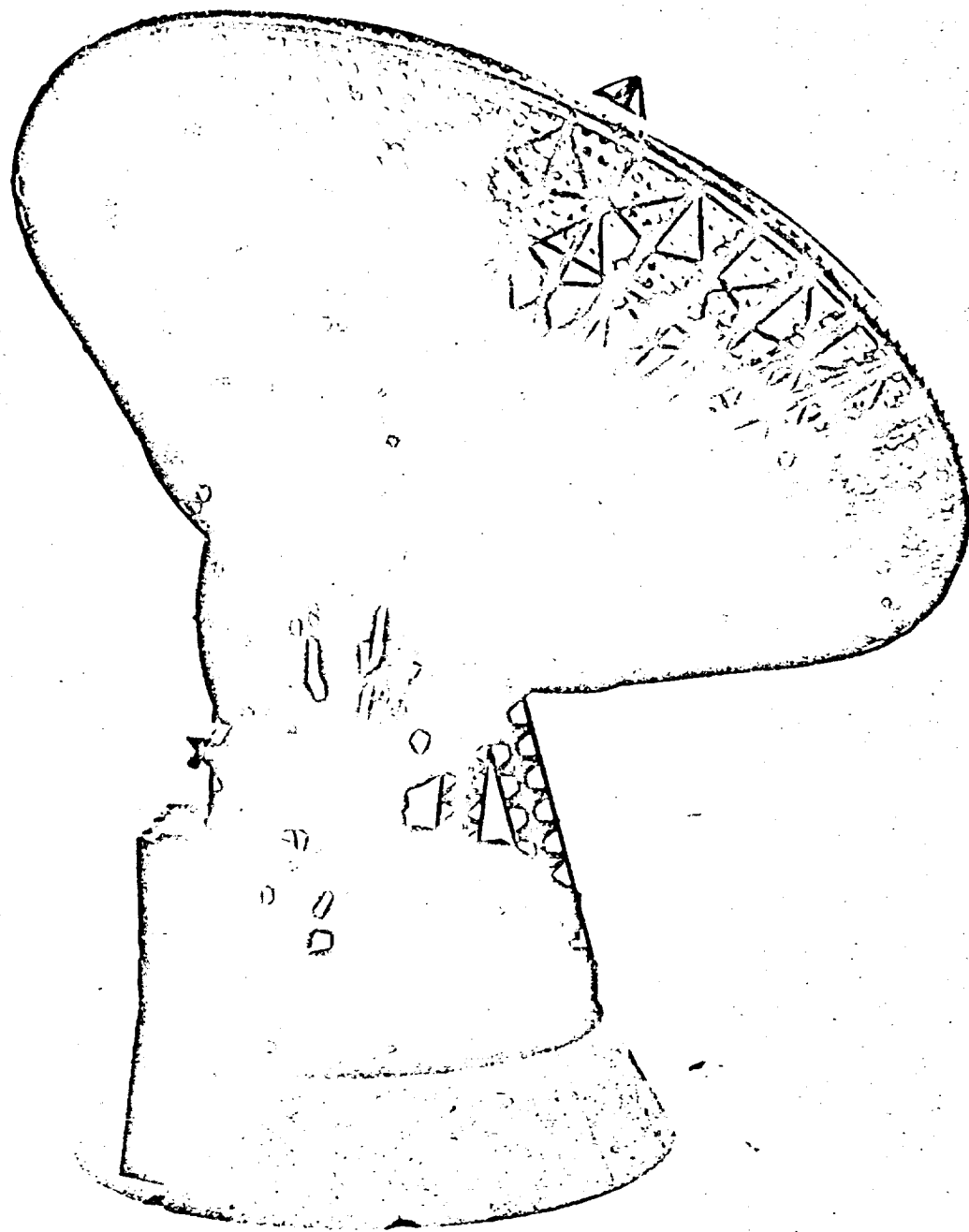


Fig. 12. Basic configuration with cone base

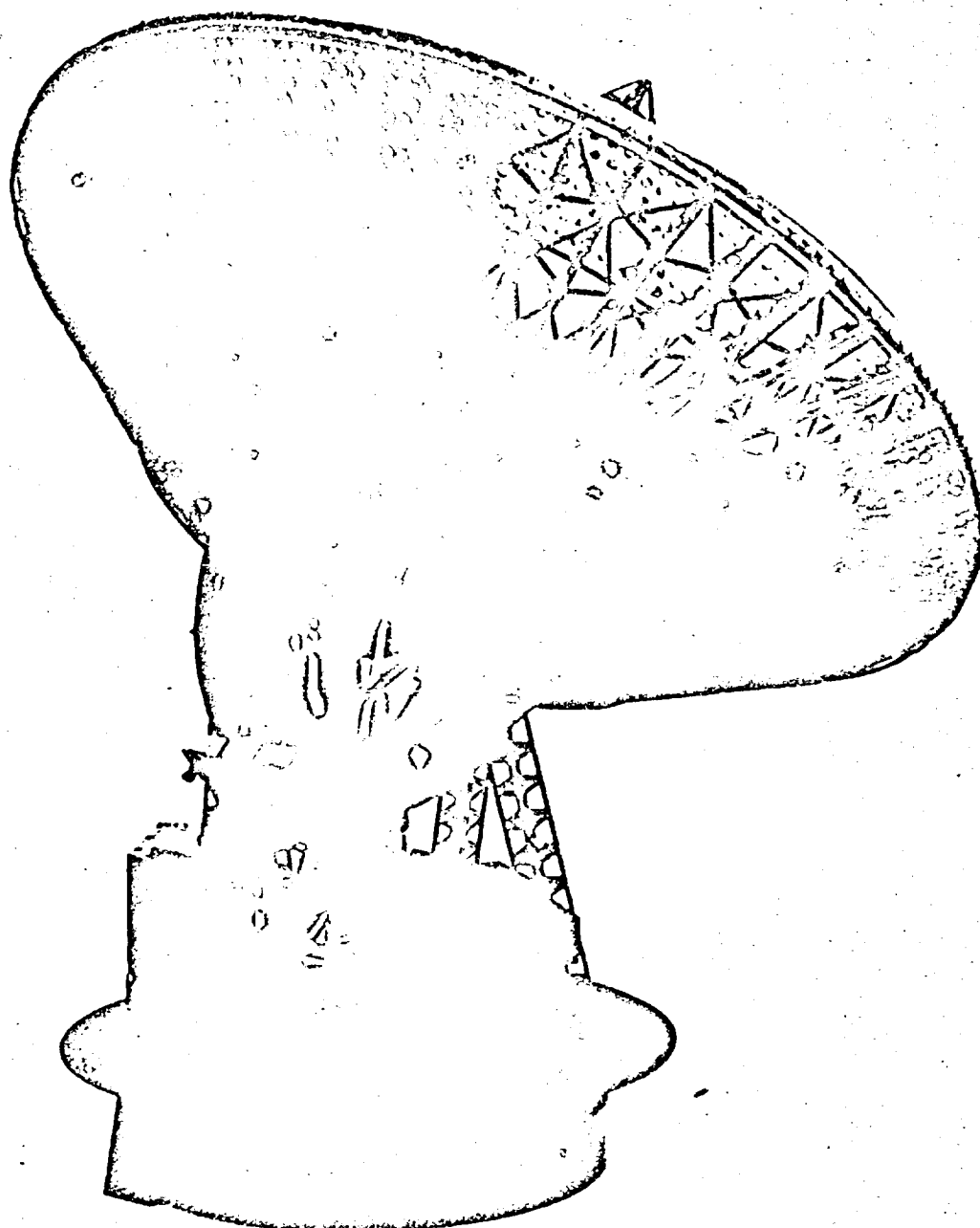


Fig. 13. Basic configuration with wind up-flow shield on cylinder base

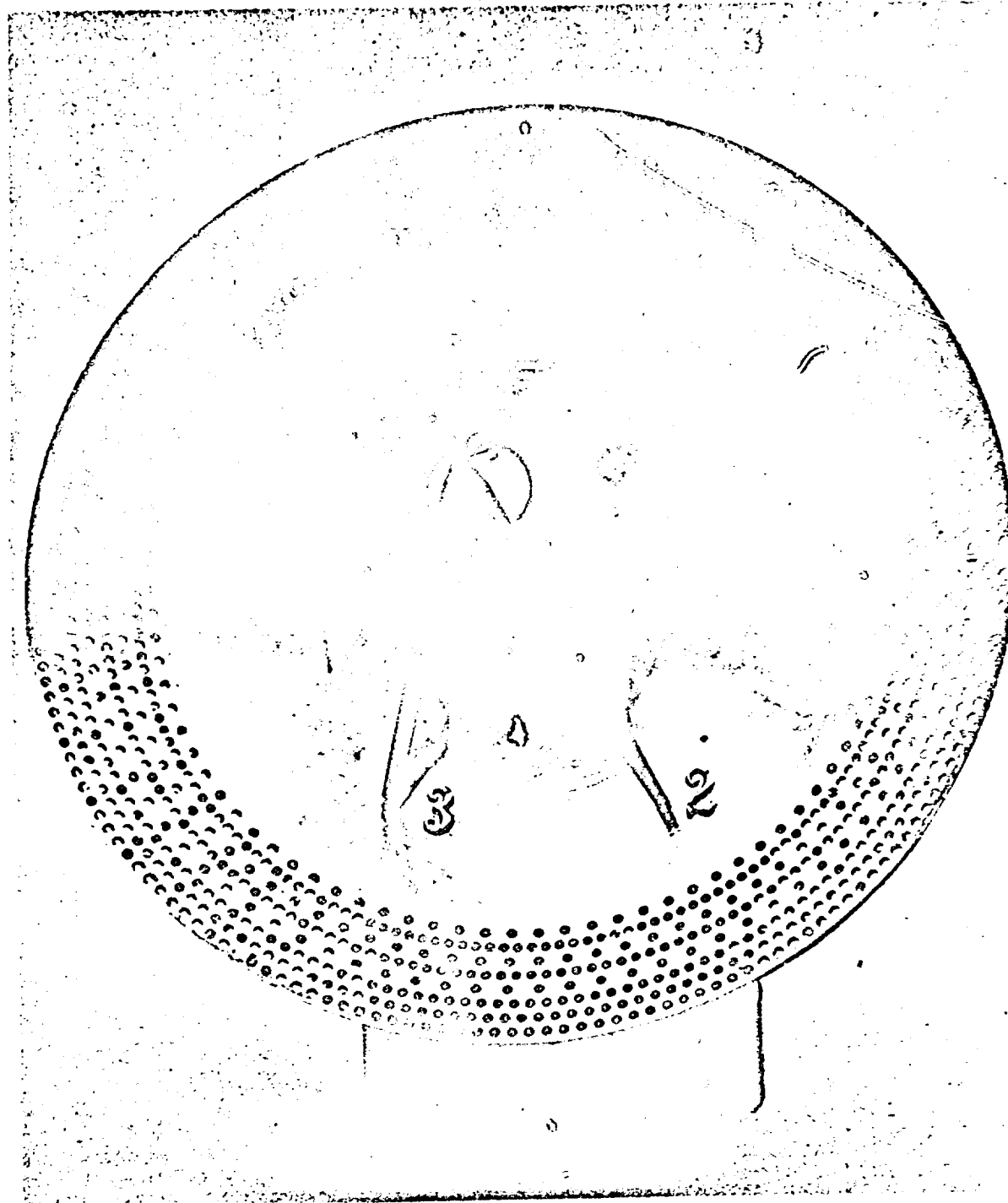


Fig. 14. Quadripod structure leg-code numbers

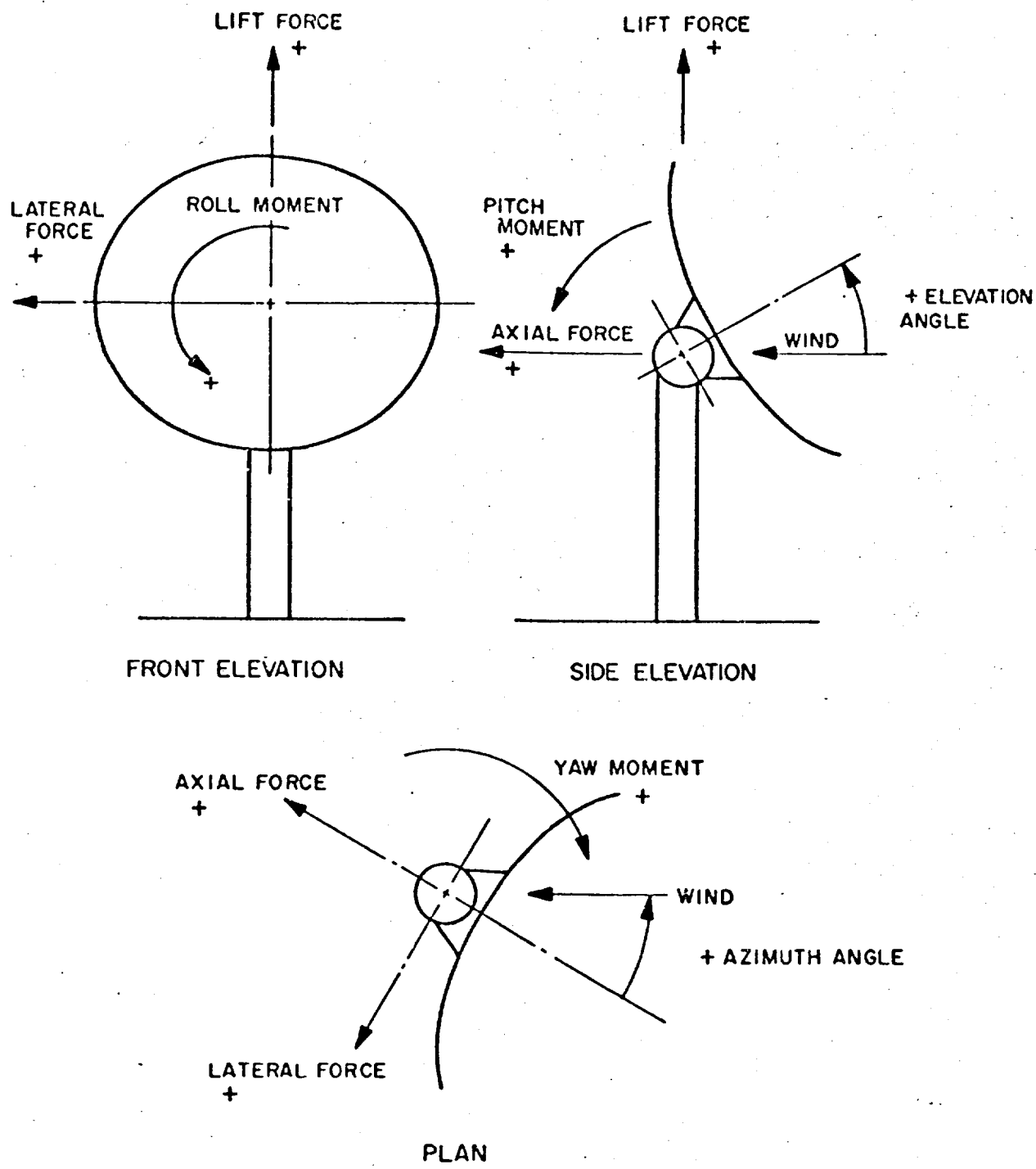


Fig. 15. Stability-axis system

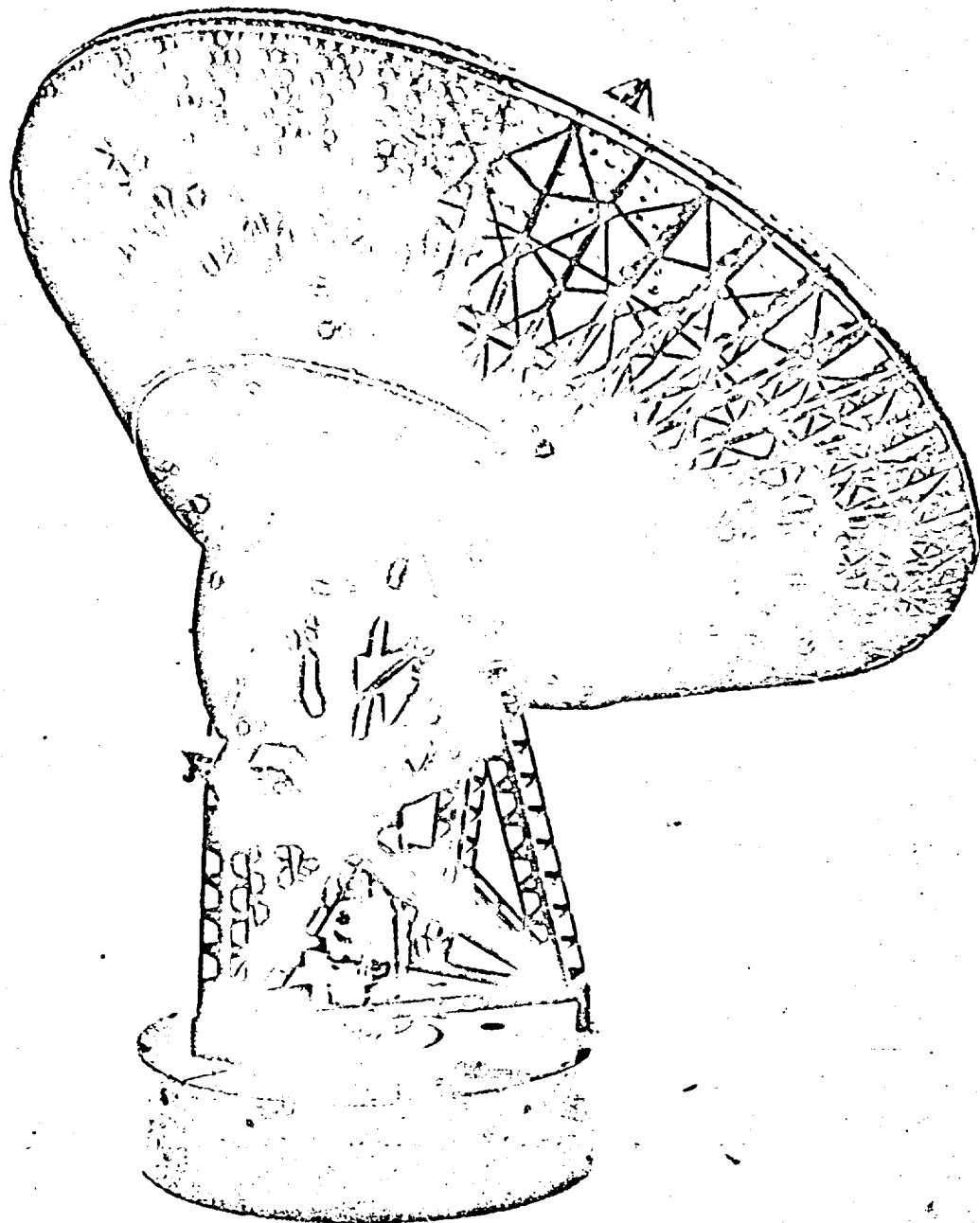


Fig. 16. Basic configuration with control rooms and elevator removed

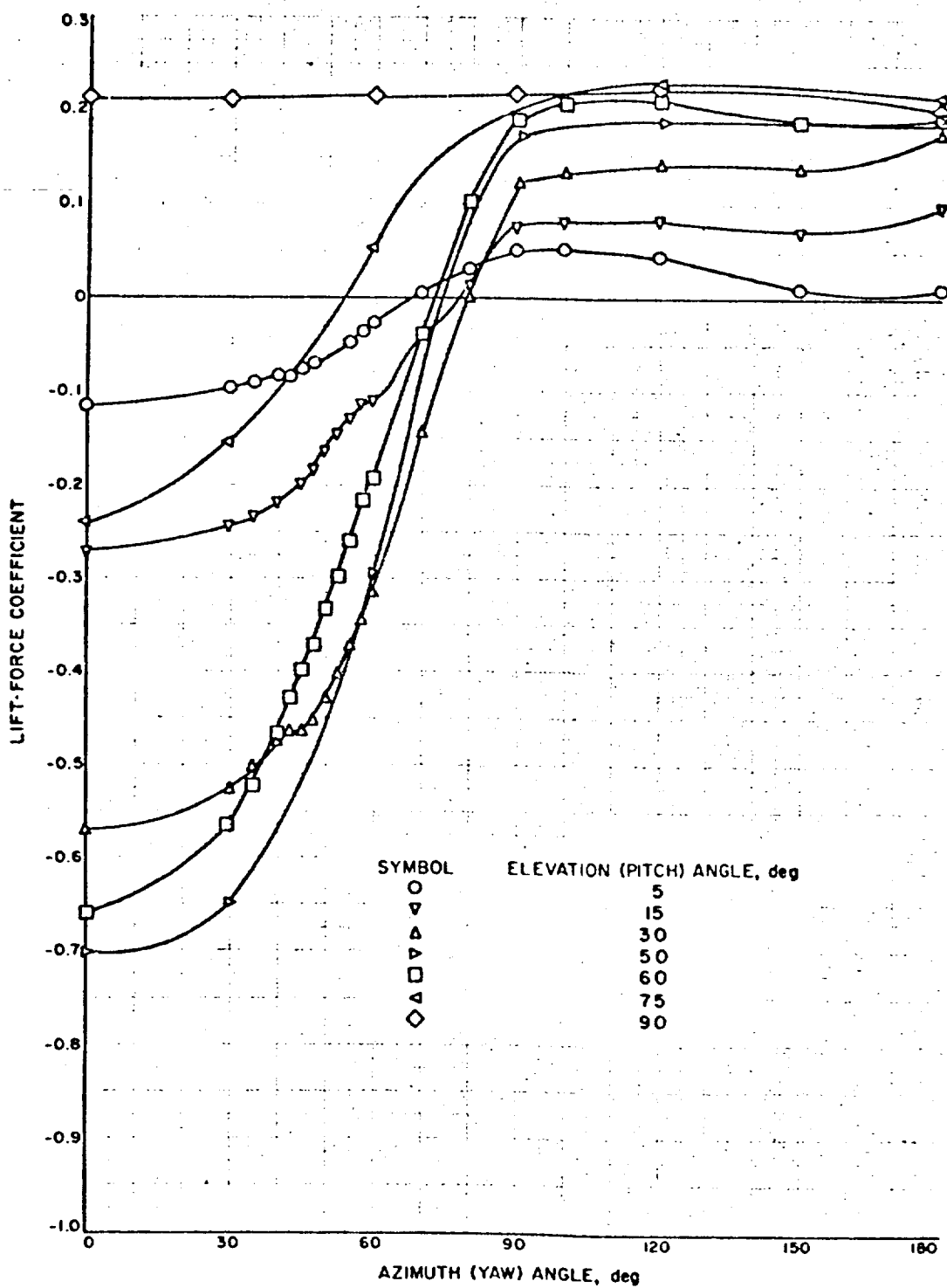


Fig. 17. Effect of antenna attitude on lift-force coefficient

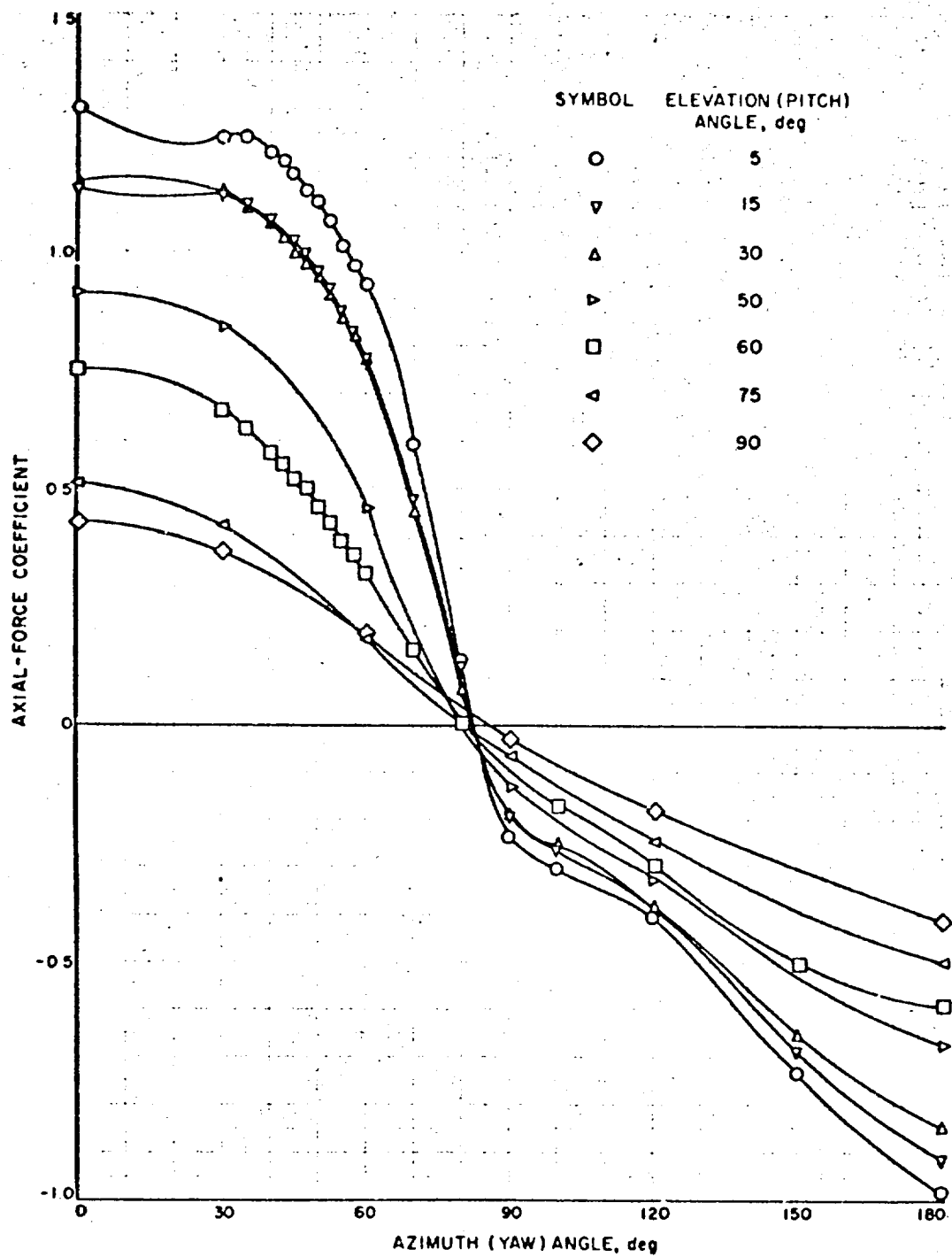


Fig. 18. Effect of antenna attitude on axial-force coefficient

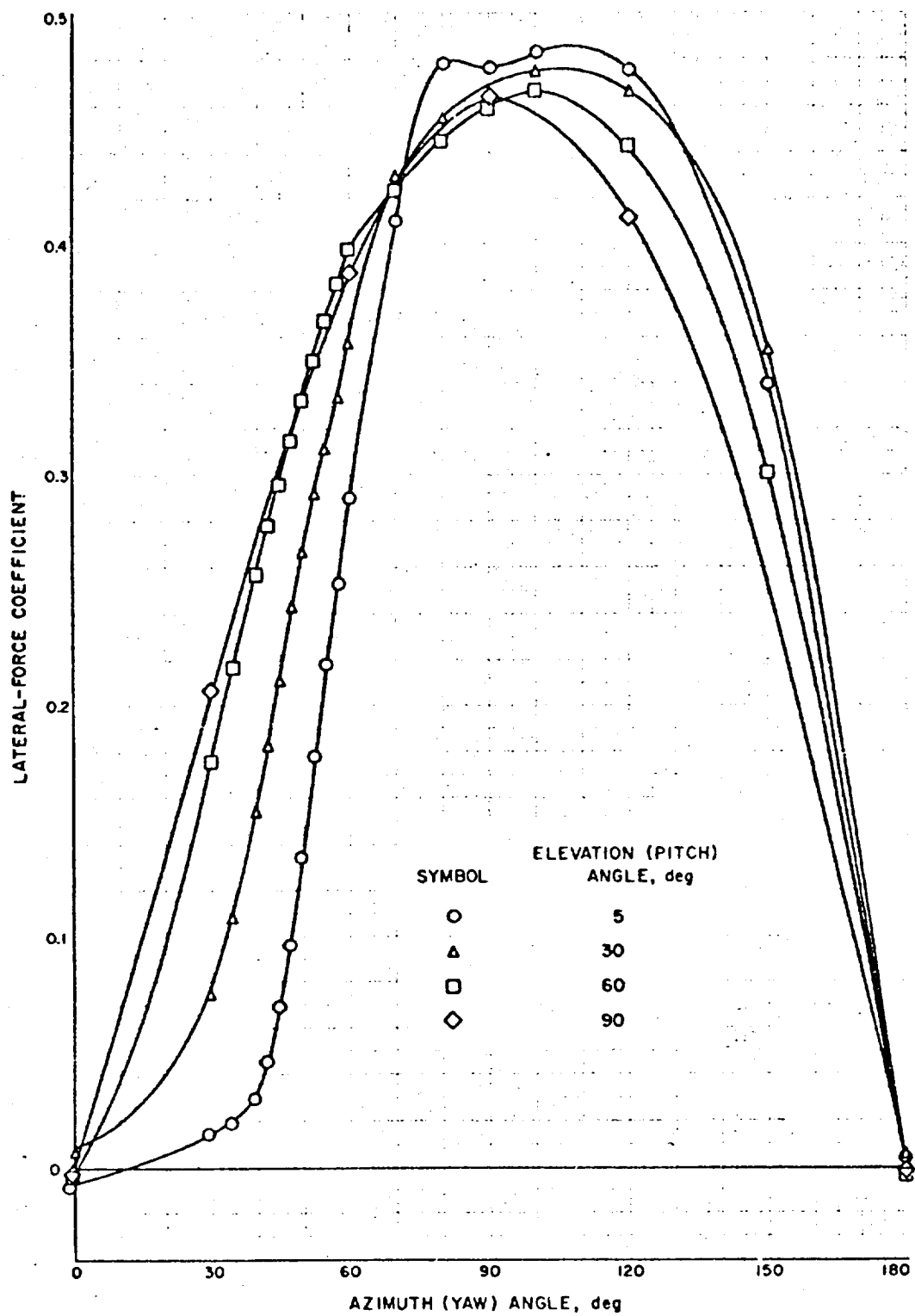


Fig. 19. Effect of antenna attitude on lateral-force coefficient

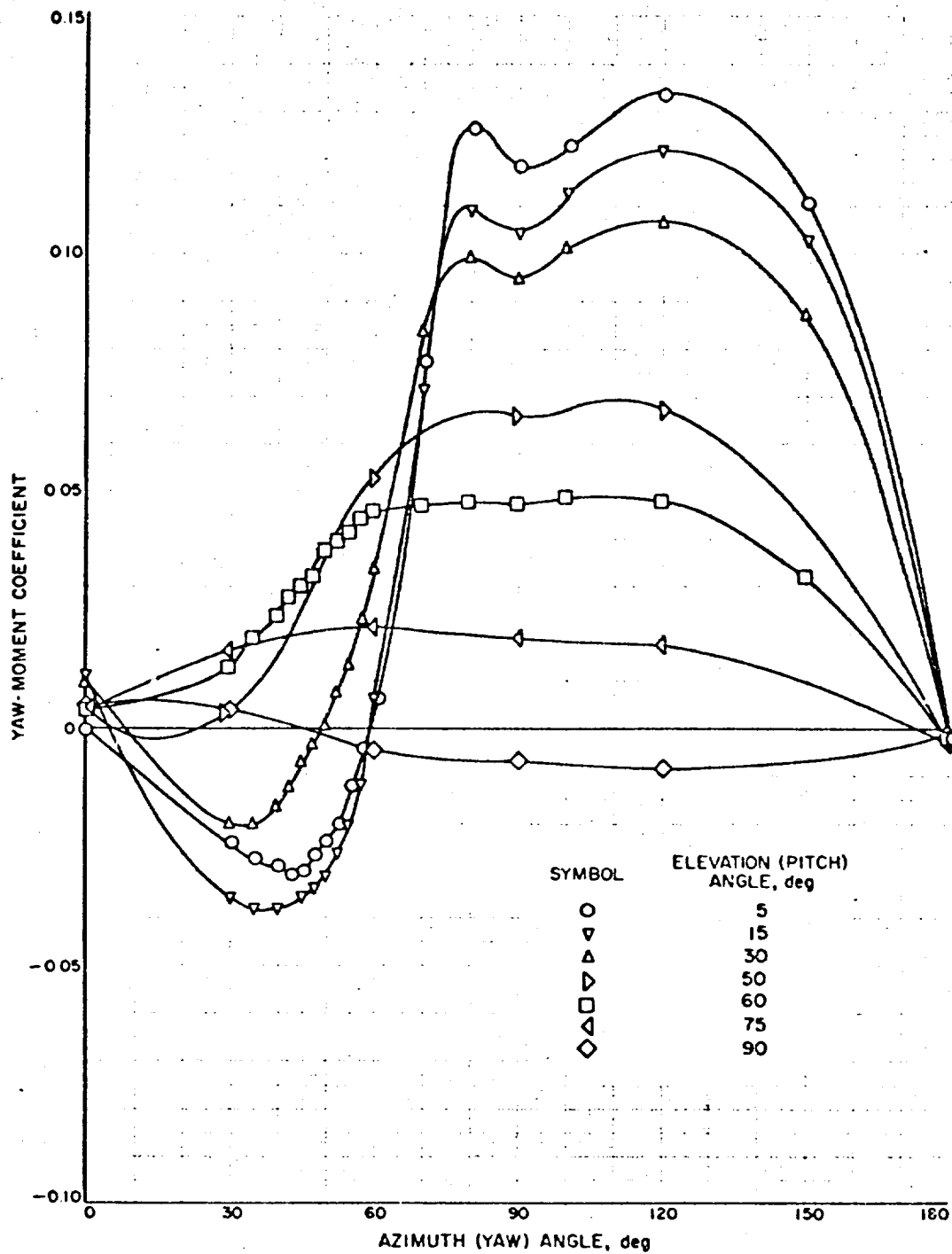


Fig. 20. Effect of antenna attitude on yaw-moment coefficient

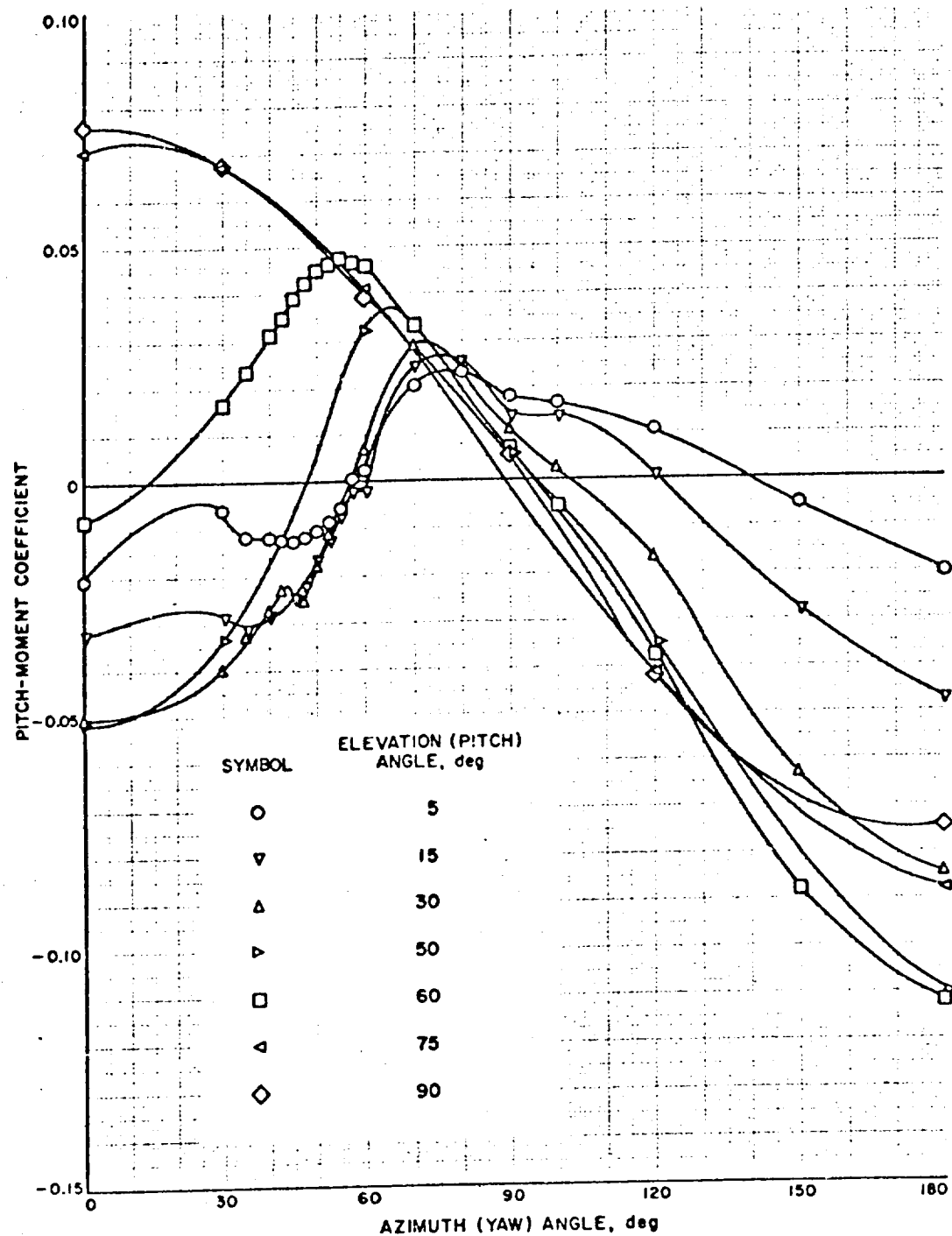


Fig. 21. Effect of antenna attitude on pitch-moment coefficient

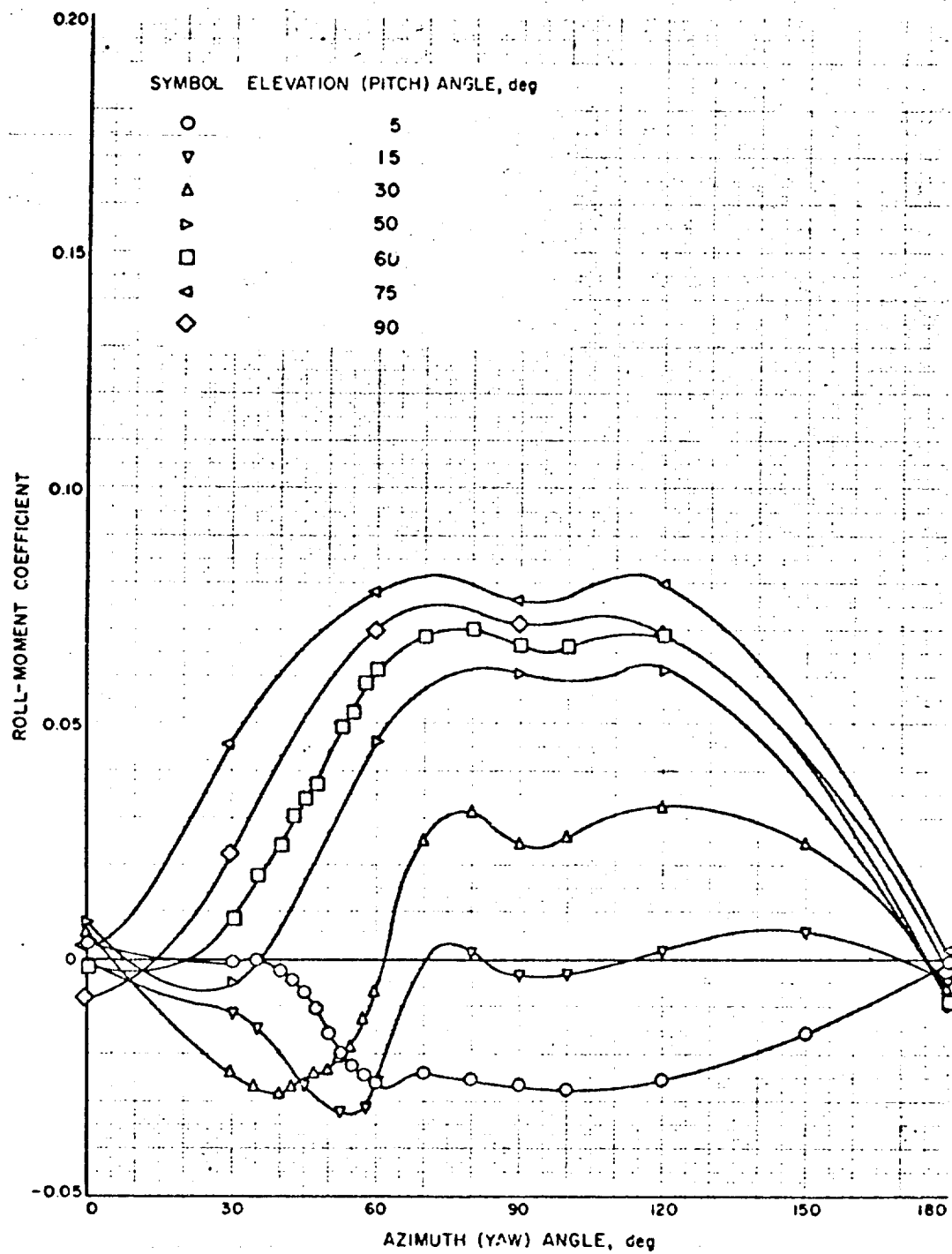


Fig. 22. Effect of antenna attitude on roll-moment coefficient

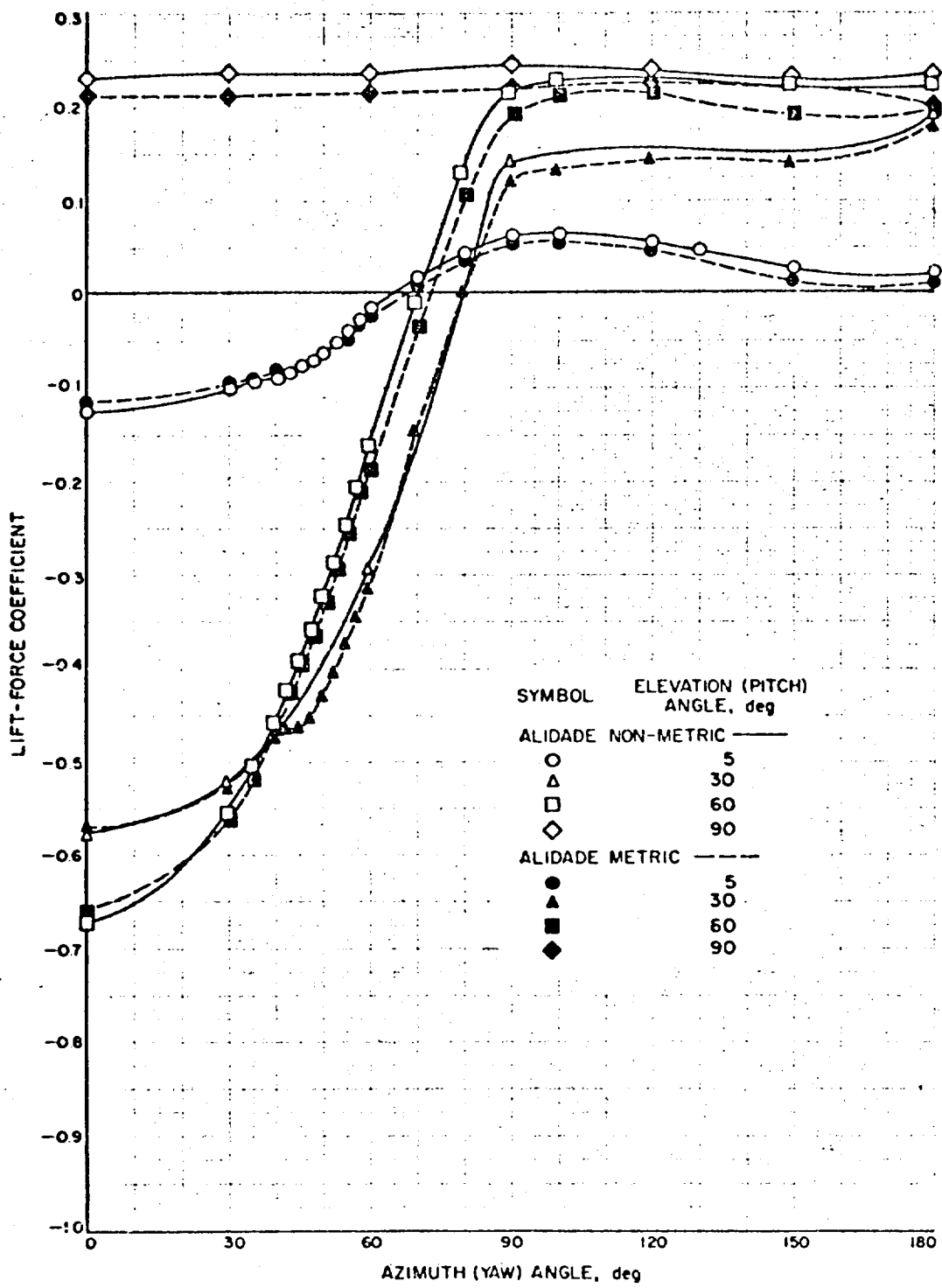


Fig. 23. Contributions of alidade on lift-force coefficient

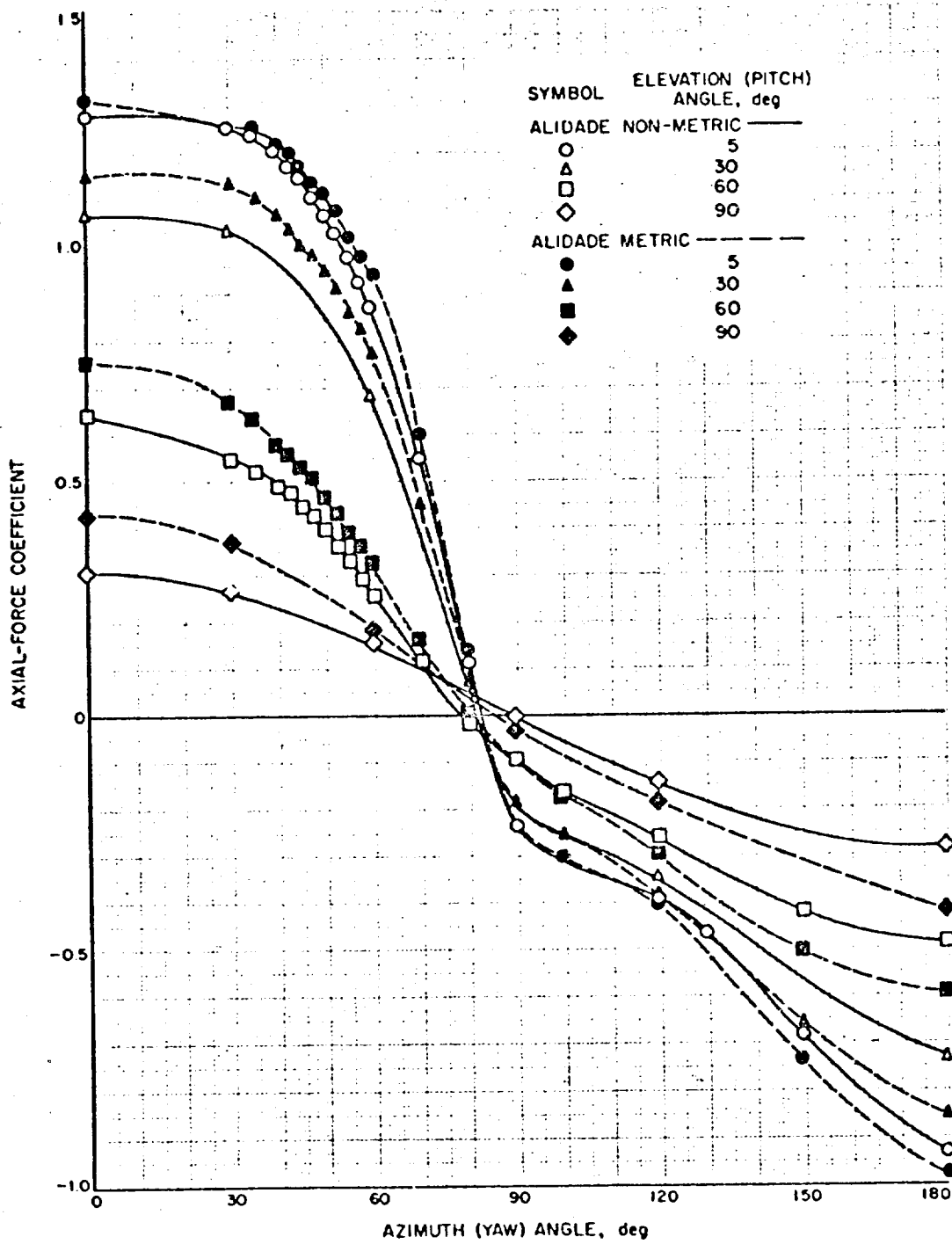


Fig. 24. Contributions of alidade on axial-force coefficient

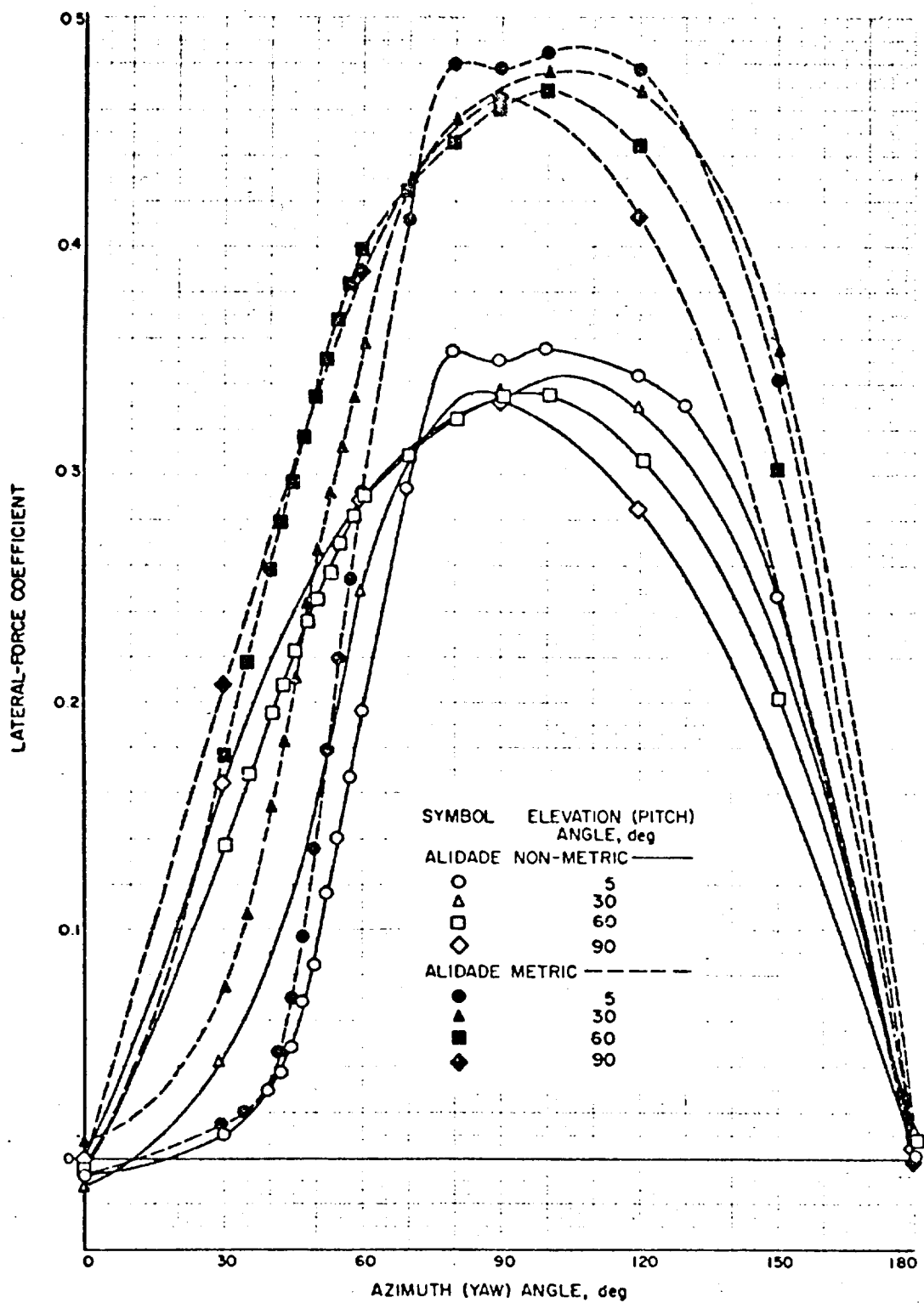


Fig. 25. Contributions of alidade on lateral-force coefficient

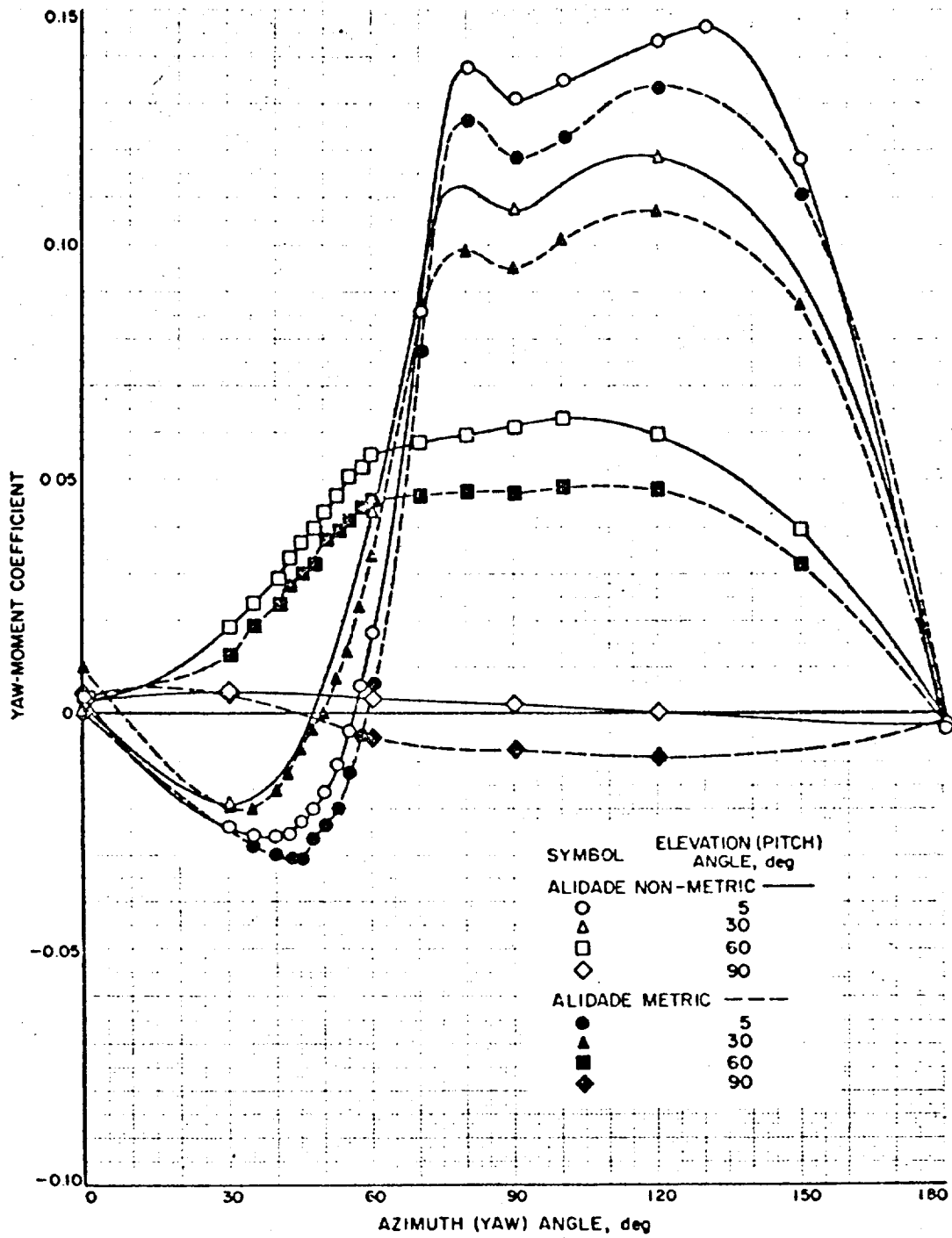


Fig. 26. Contributions of alidade on yaw-moment coefficient

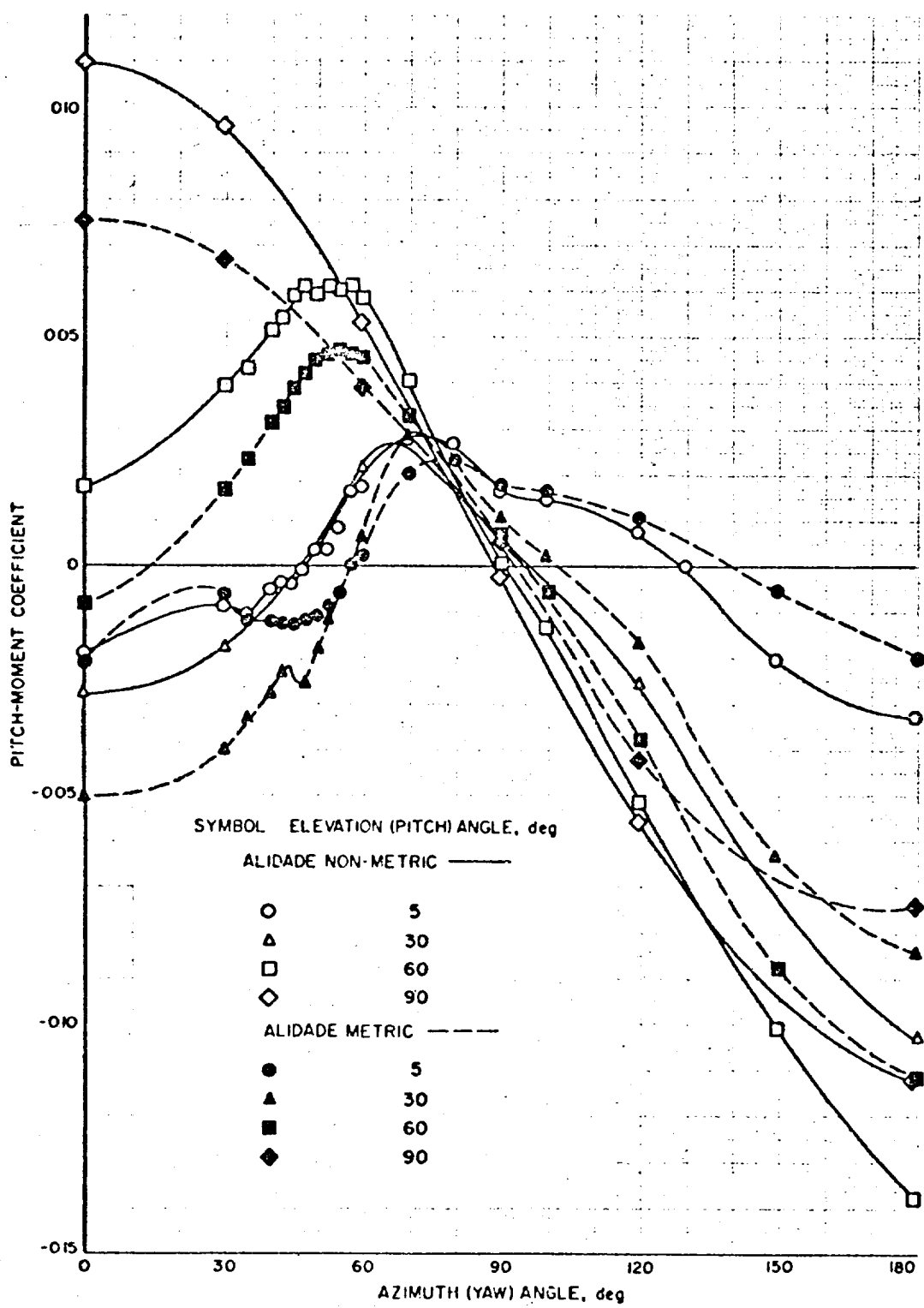


Fig. 27. Contributions of alidade on pitch-moment coefficient

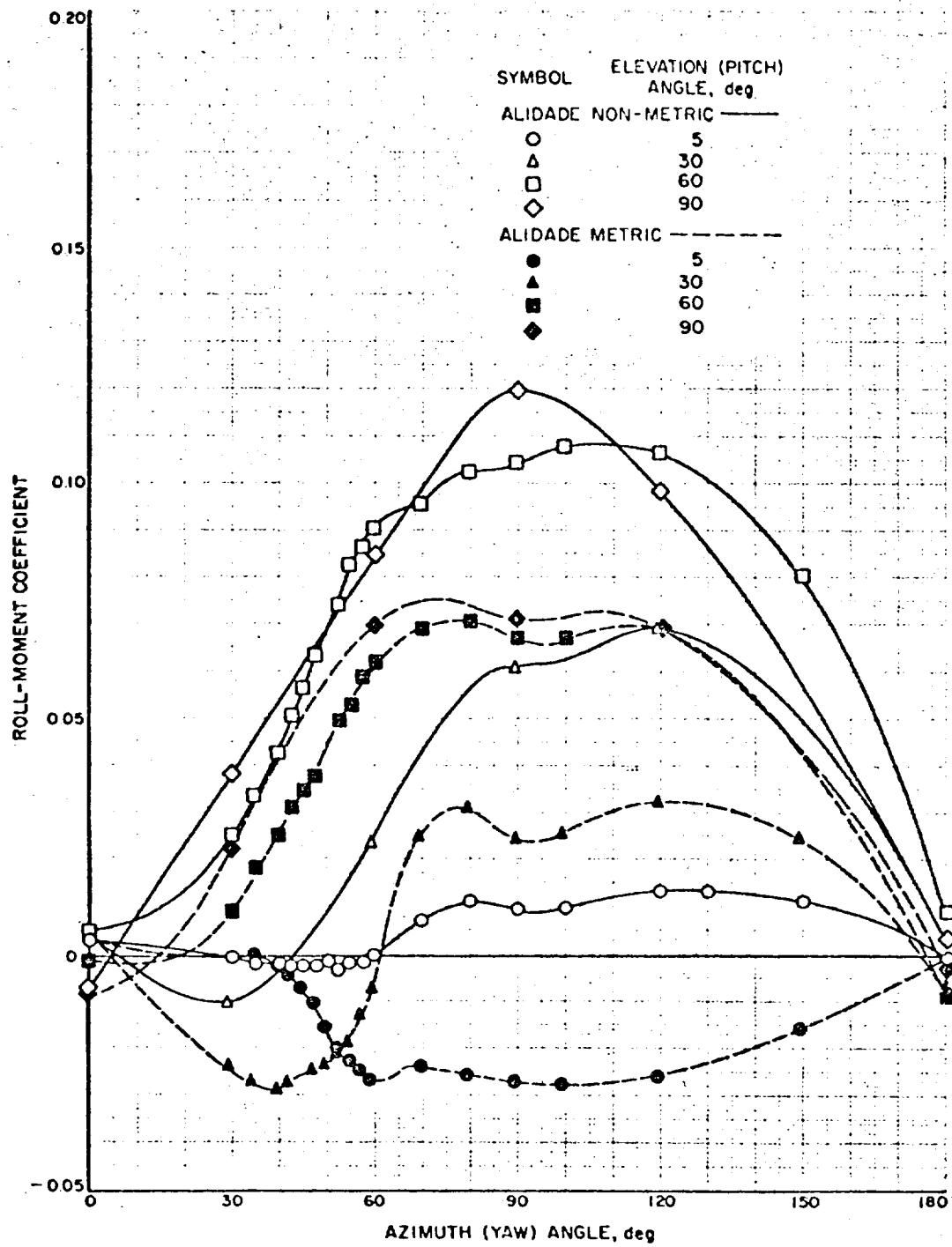


Fig. 28. Contributions of alidade on roll-moment coefficient

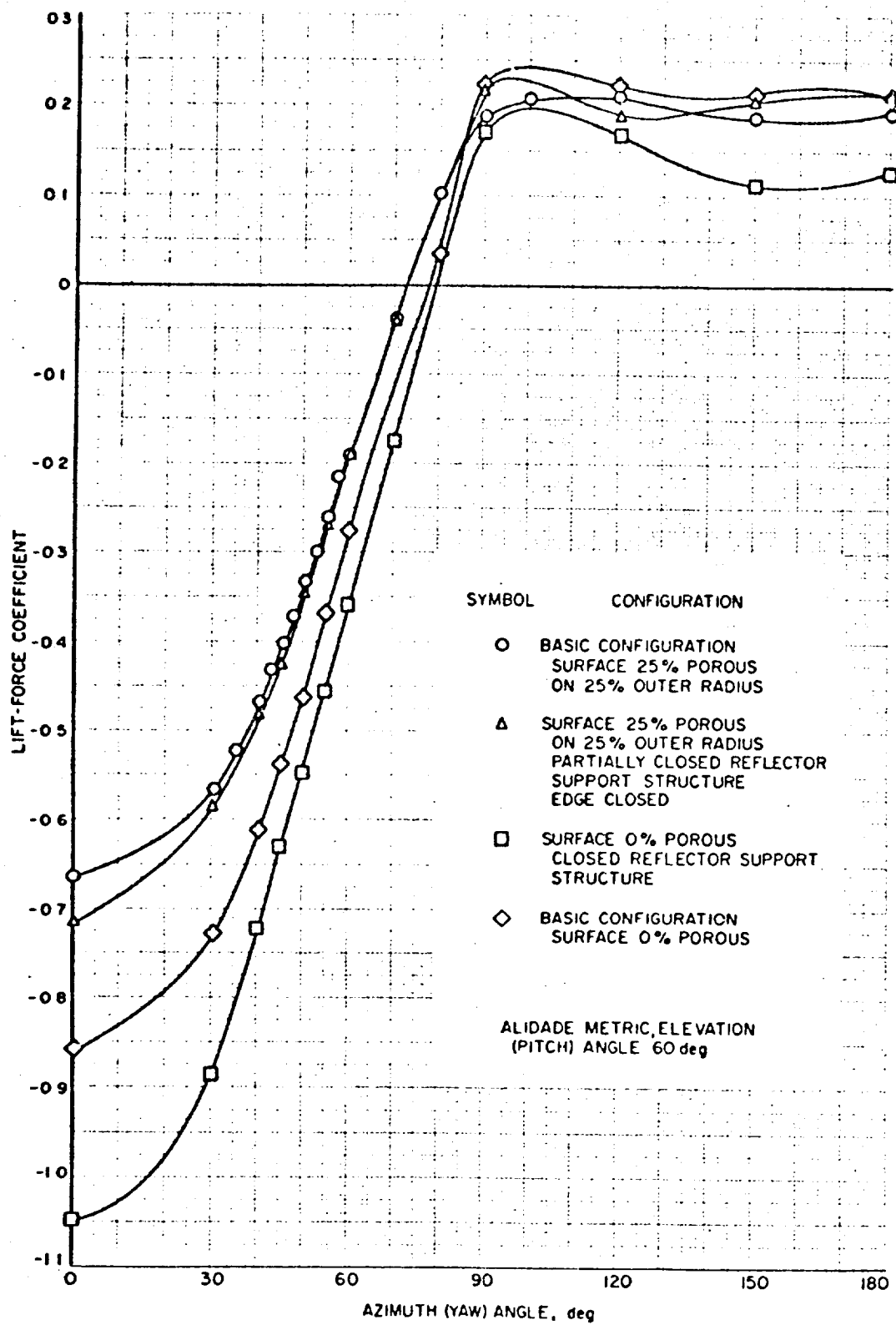


Fig. 29. Effect of changes in the reflector support structure on lift-force coefficient

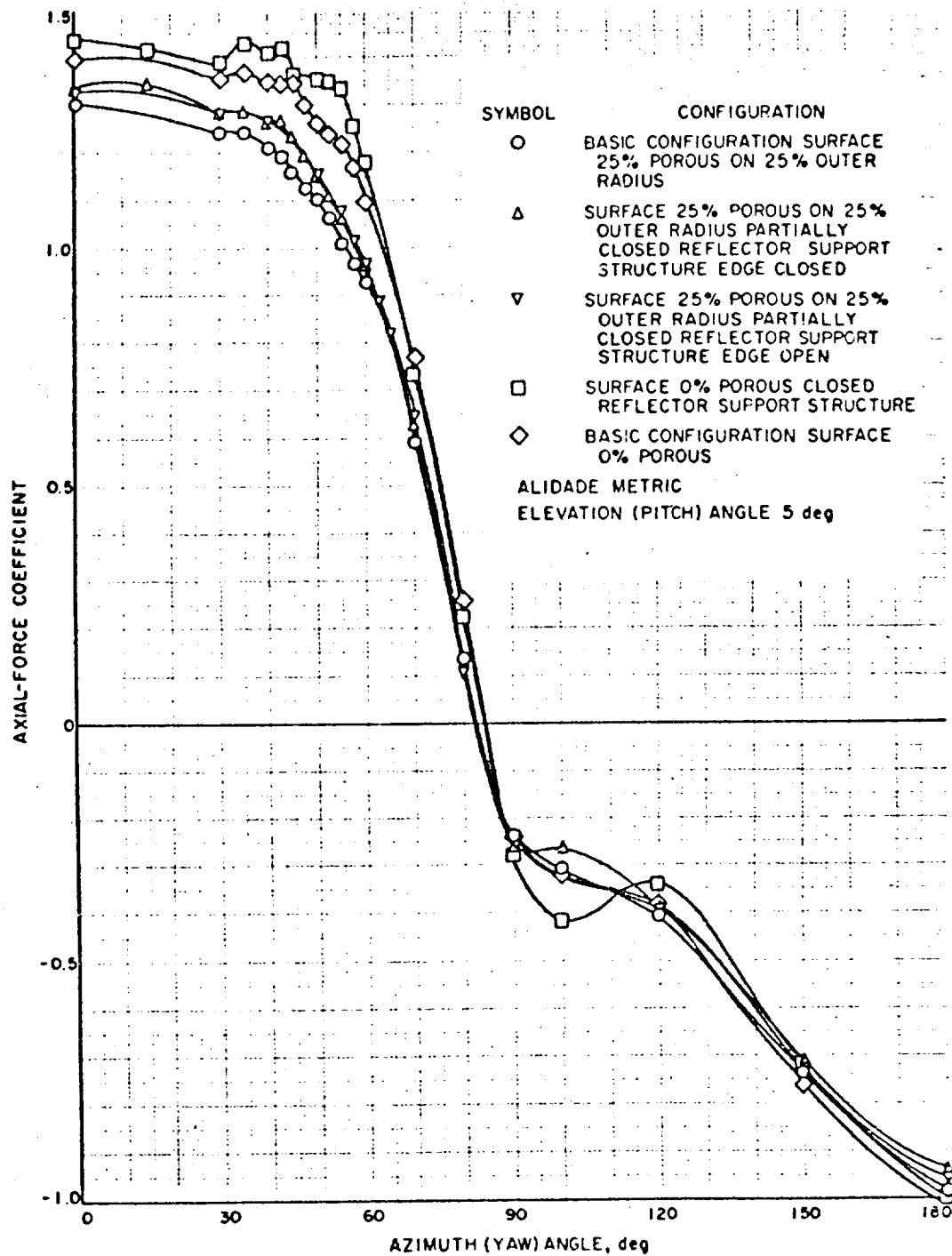


Fig. 30. Effect of changes in the reflector support structure on axial-force coefficient

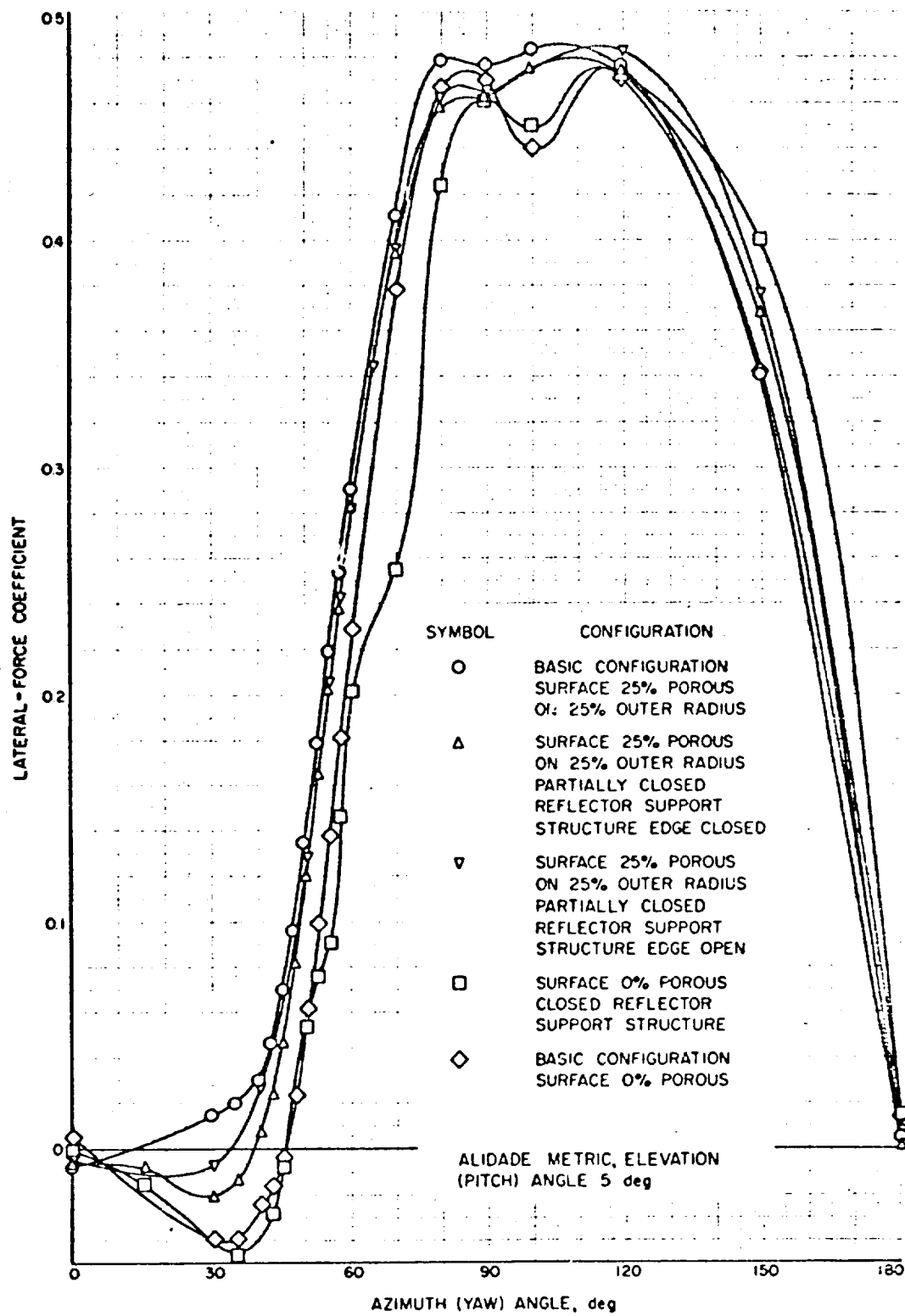


Fig. 31. Effect of changes in the reflector support structure on lateral-force coefficient

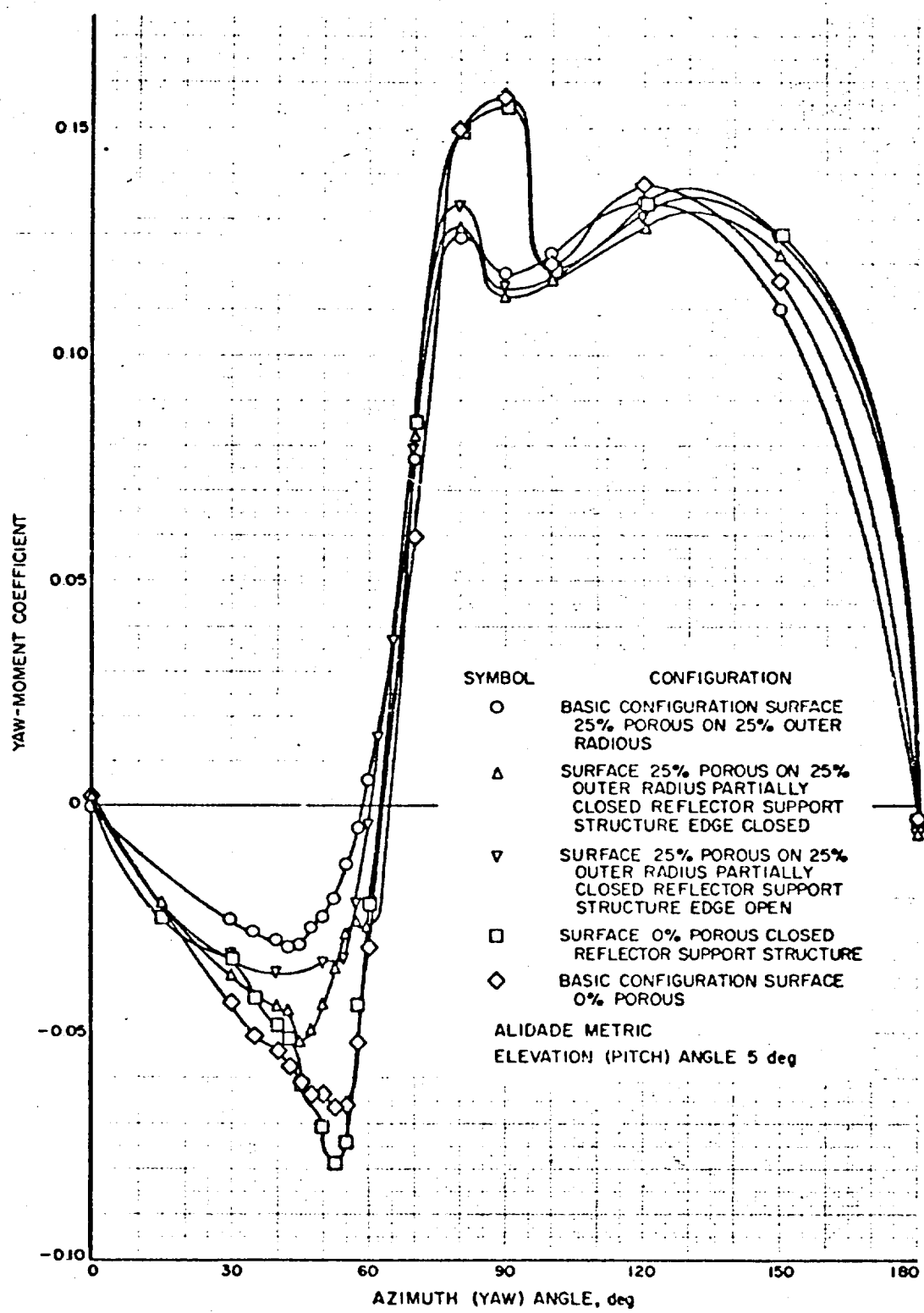


Fig. 32. Effect of changes in the reflector support structure on yaw-moment coefficient

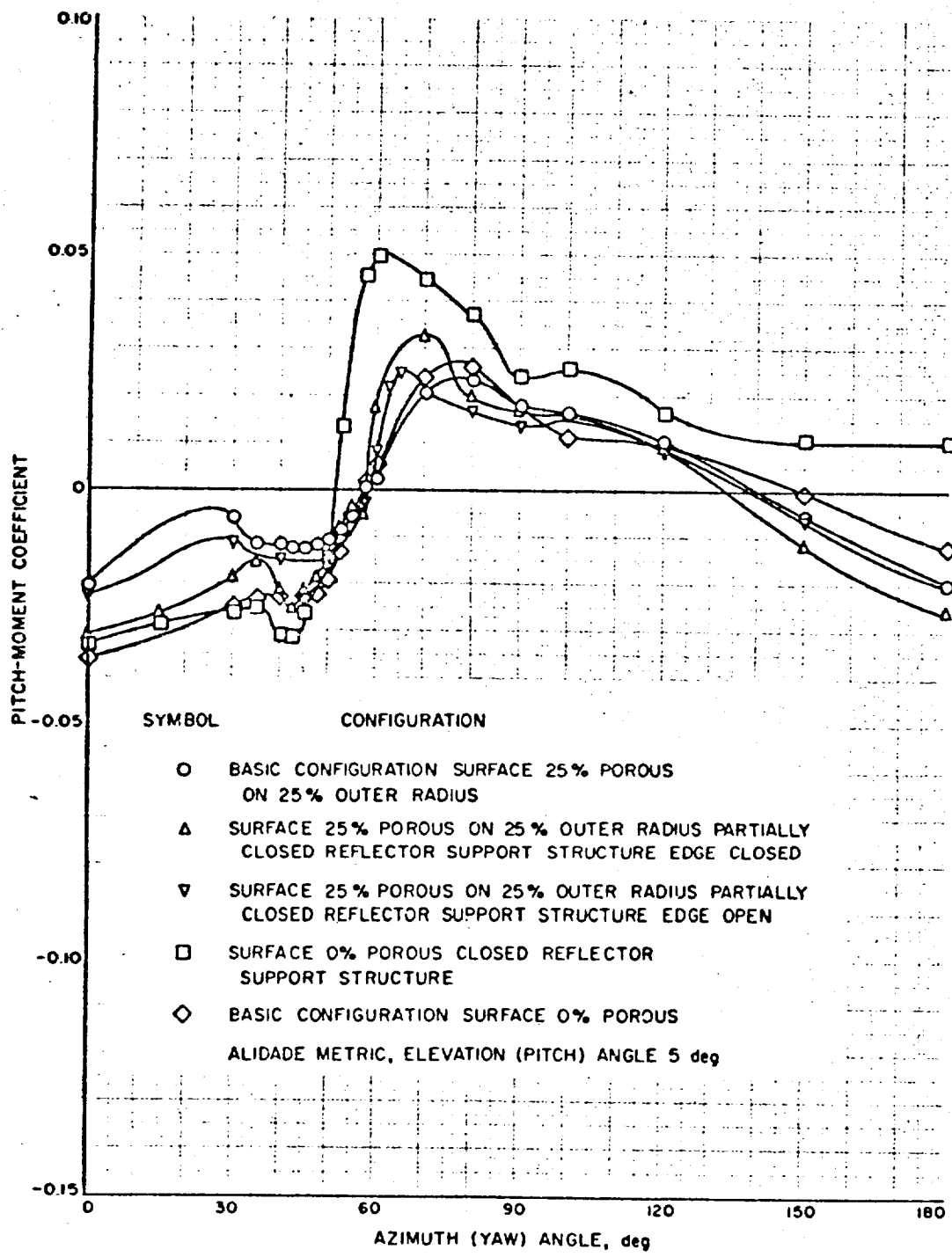


Fig. 33. Effect of changes in the reflector support structure on pitch-moment coefficient

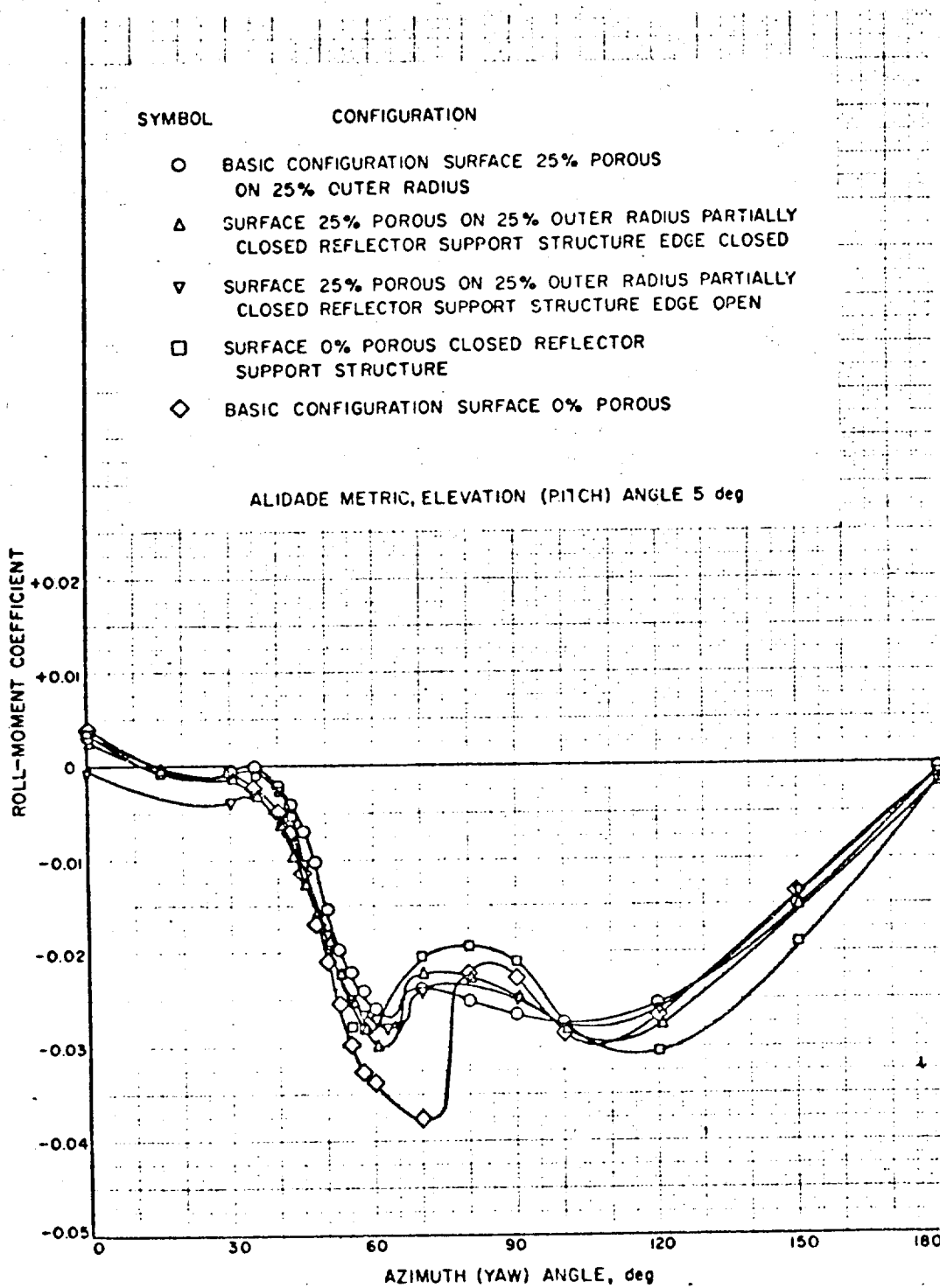


Fig. 34. Effect of changes in the reflector support structure on roll-moment coefficient

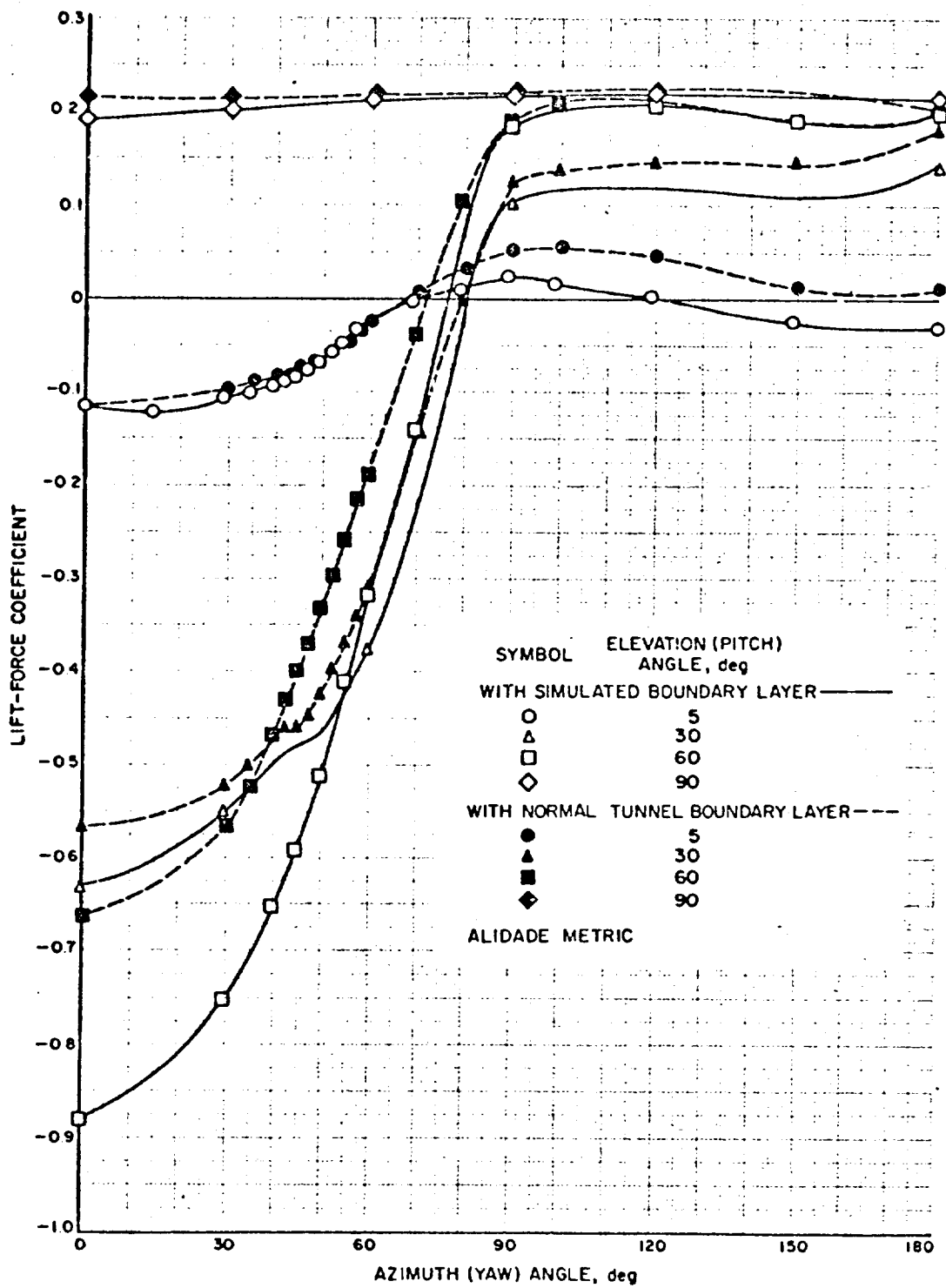


Fig. 35. Effect of velocity gradients on lift-force coefficient

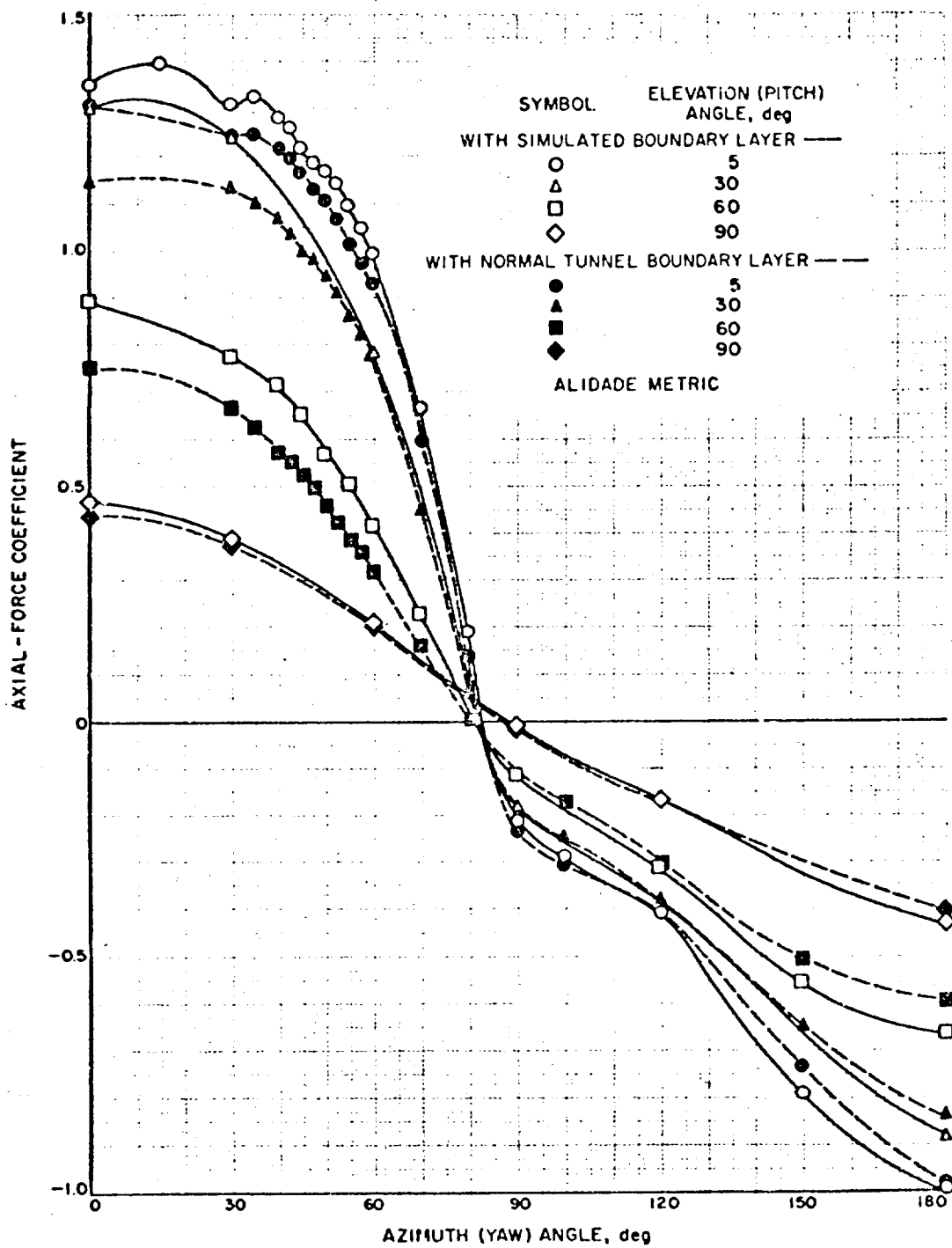


Fig. 36. Effect of velocity gradients on axial-force coefficient

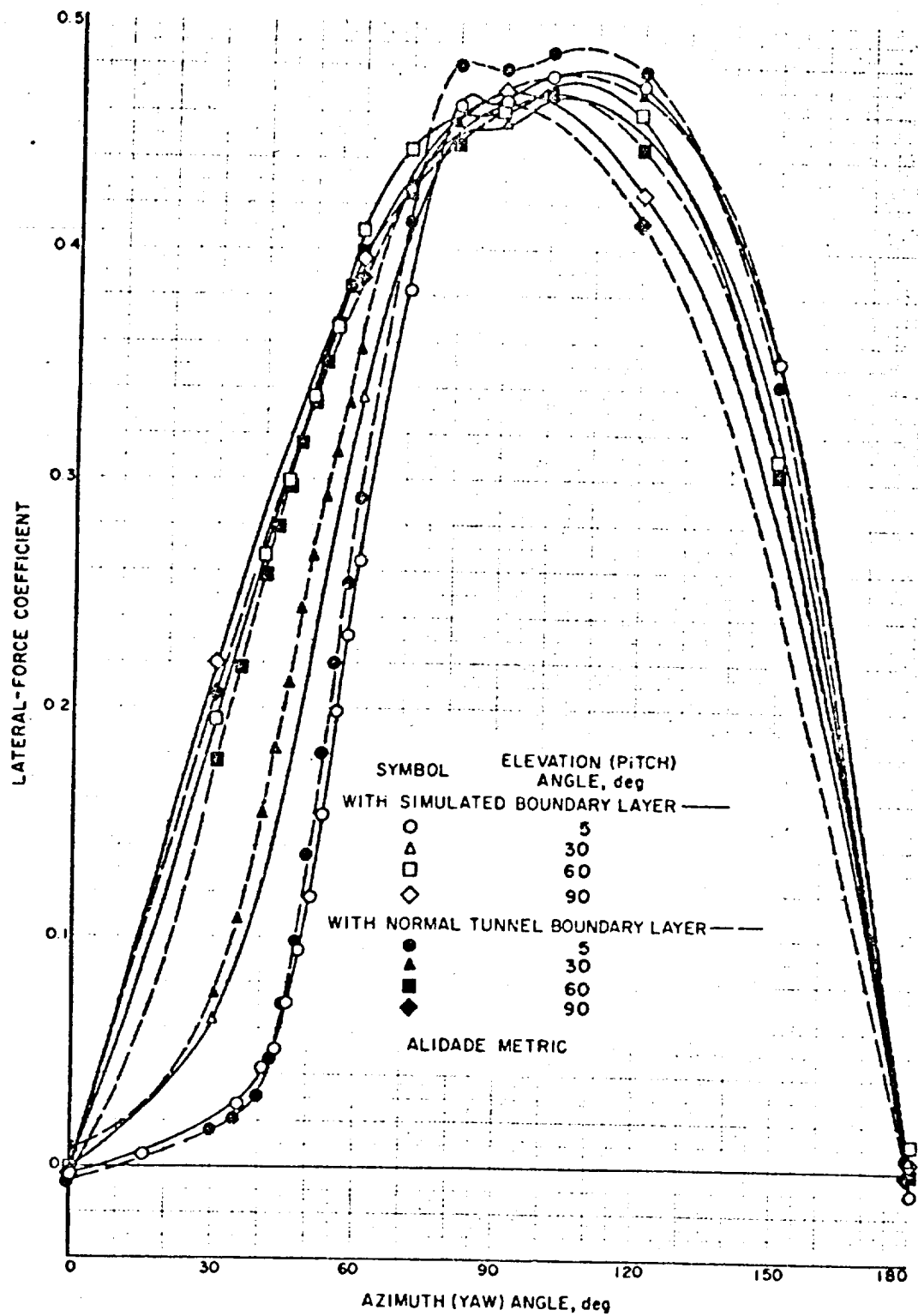


Fig. 37. Effect of velocity gradients on lateral-force coefficient

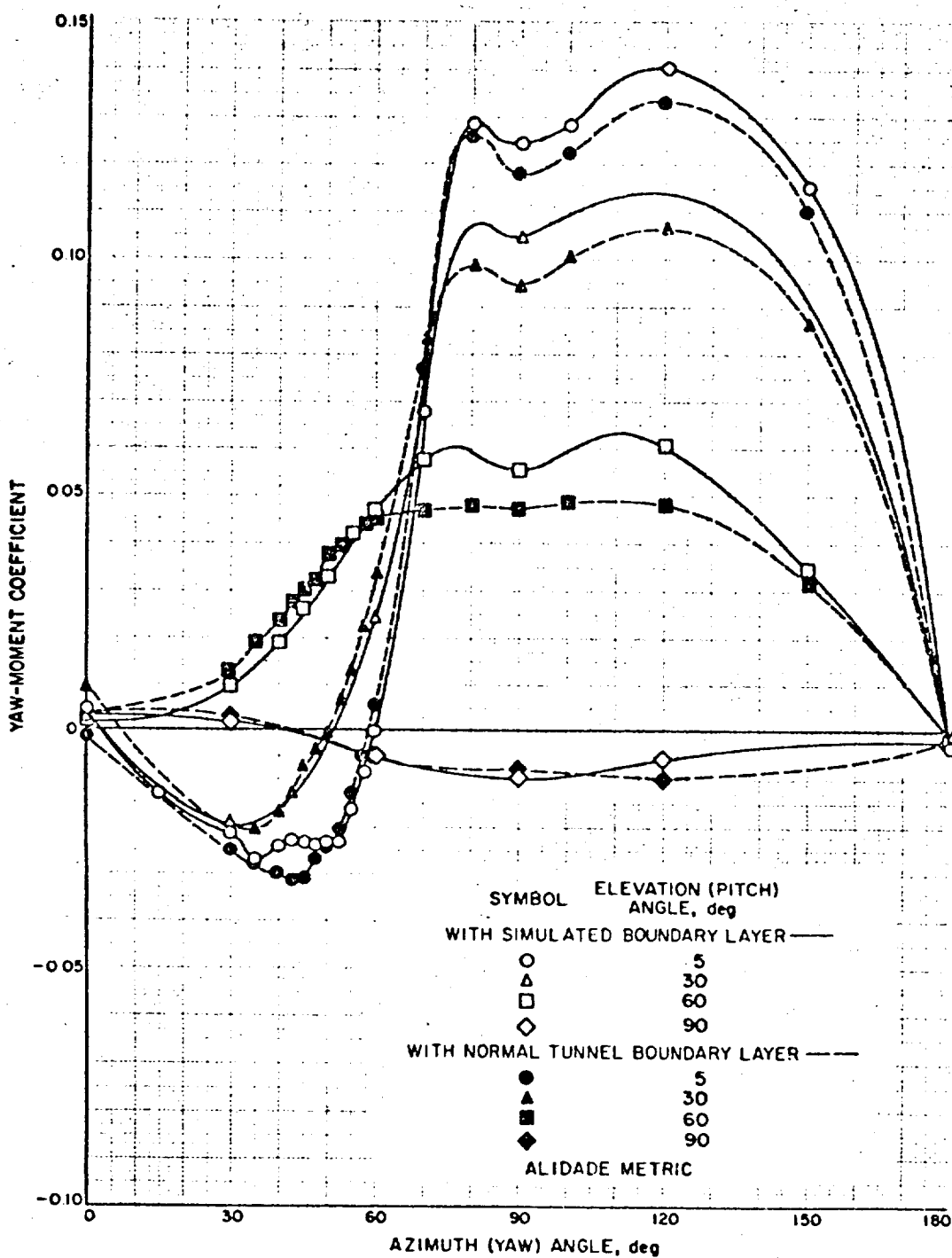


Fig. 38. Effect of velocity gradients on yaw-moment coefficient

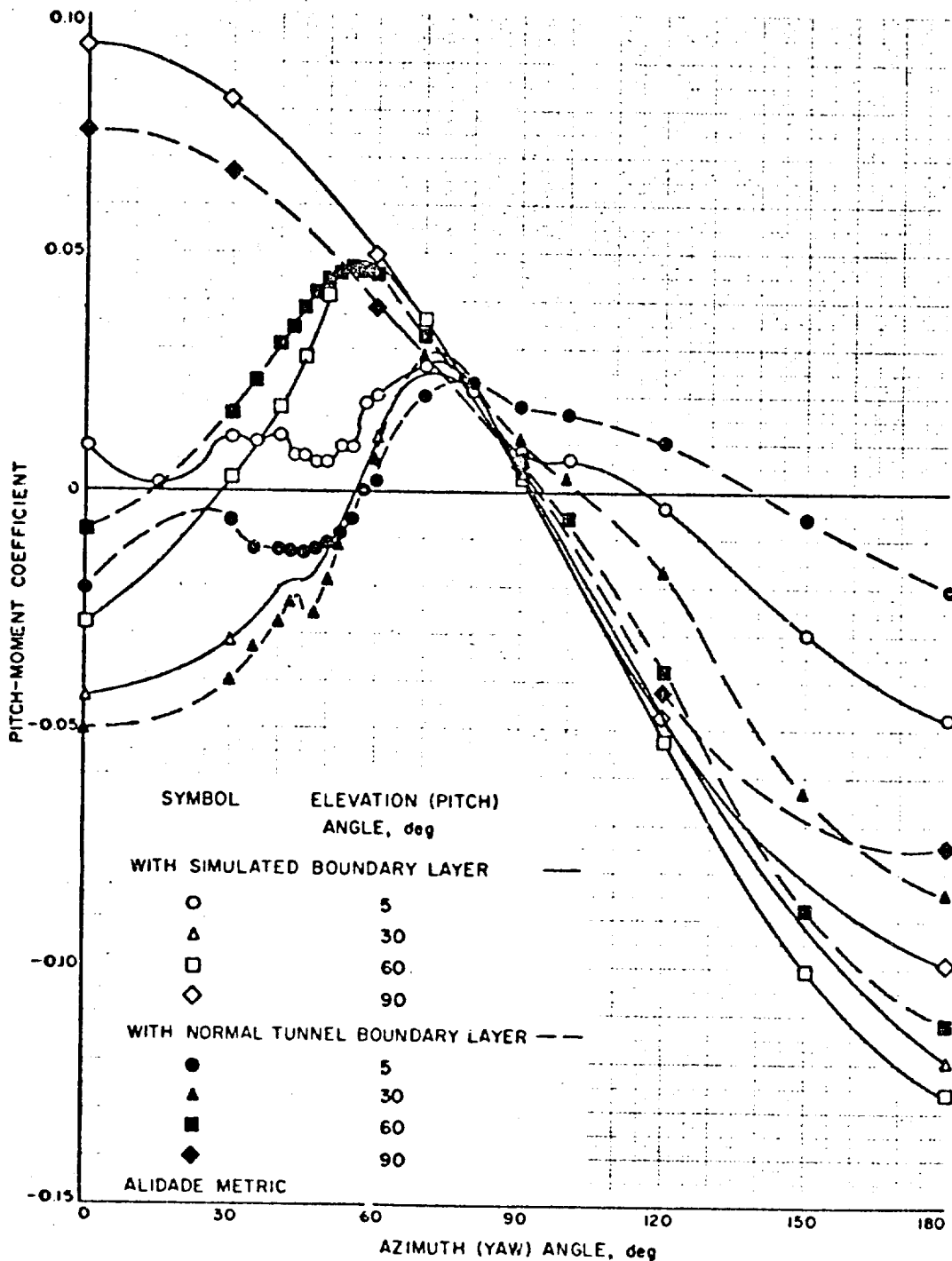


Fig. 39. Effect of velocity gradients on pitch-moment coefficient

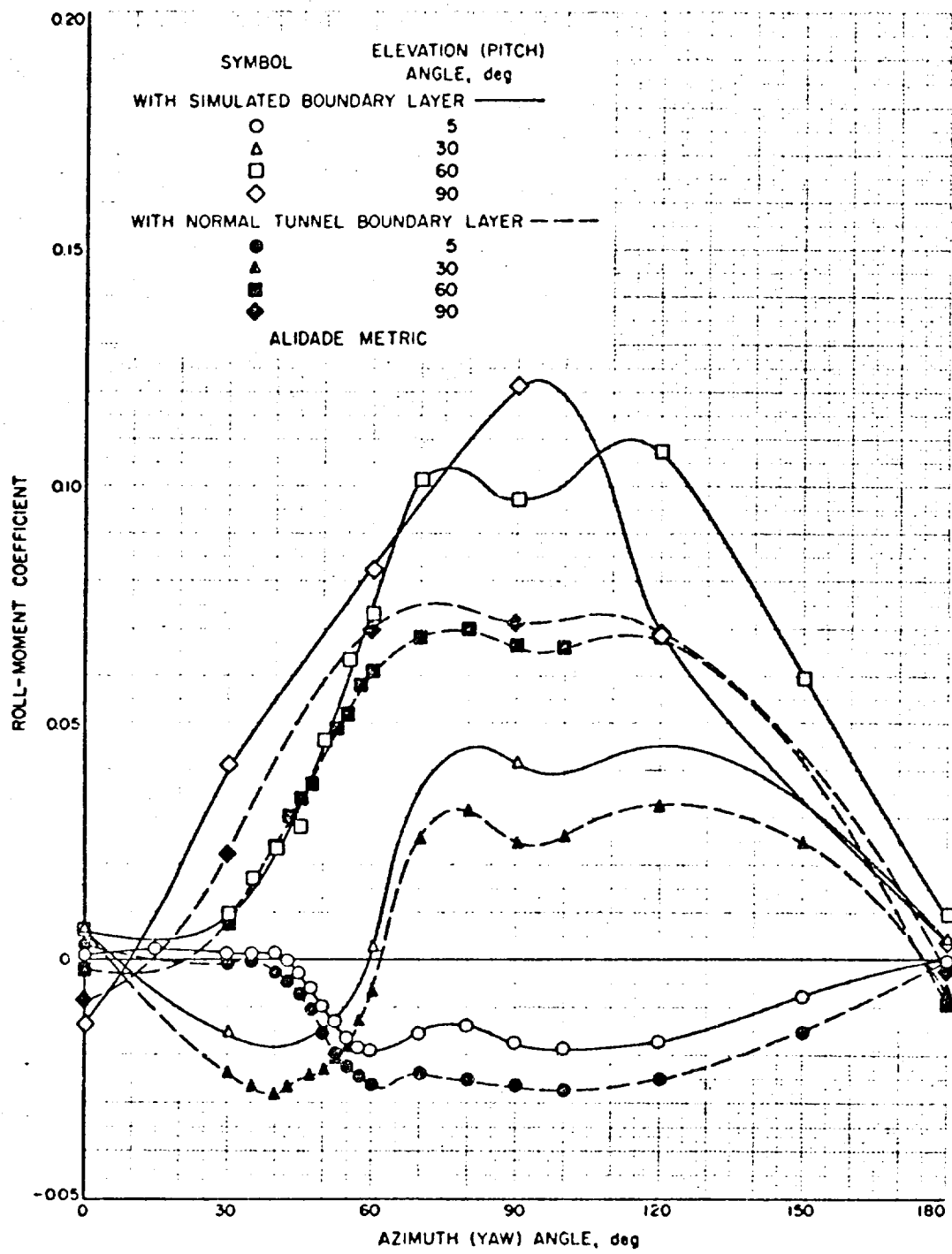


Fig. 40. Effect of velocity gradients on roll-moment coefficient

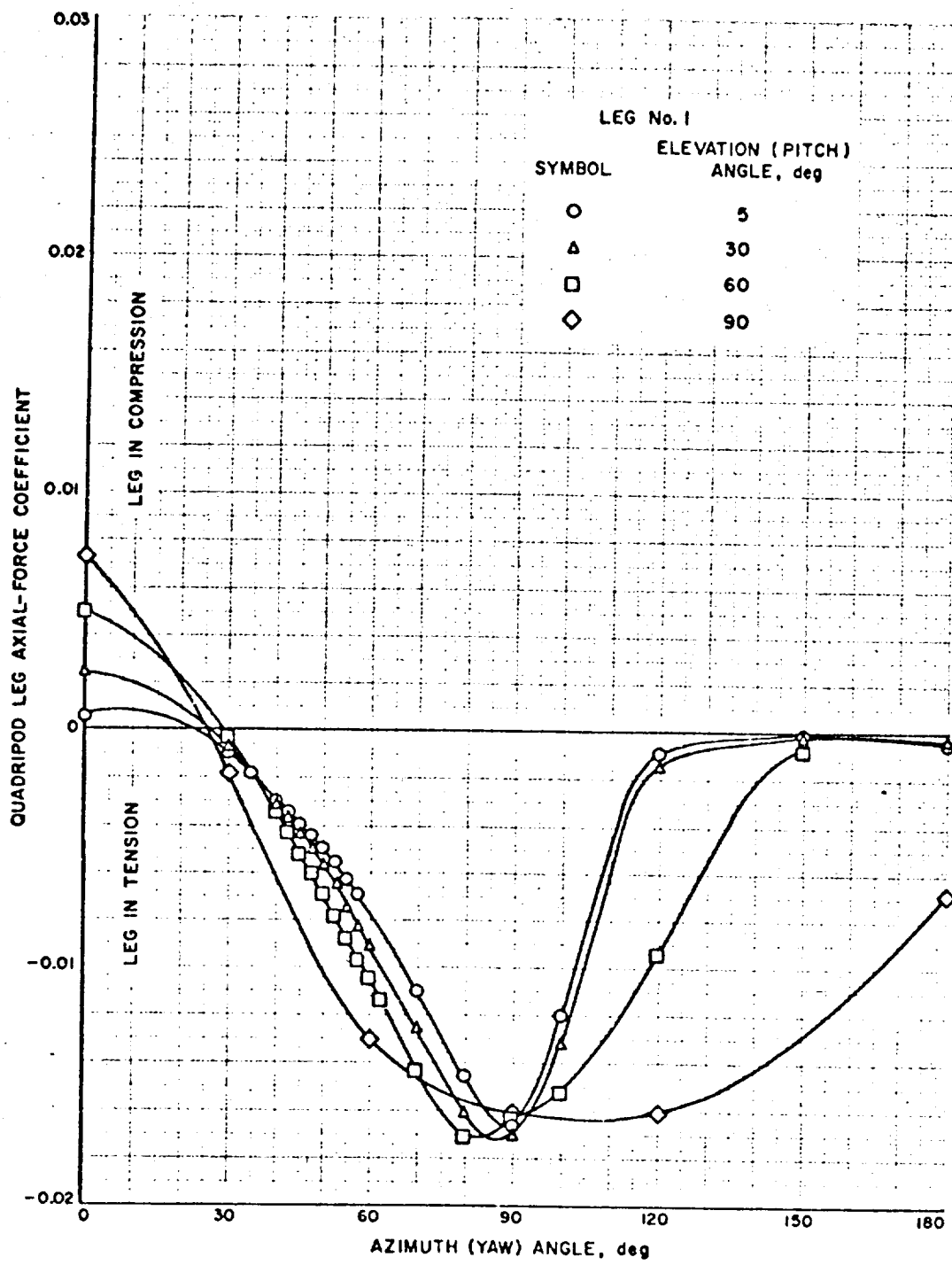


Fig. 41. Axial-force coefficient on leg 1 of quadripod structure

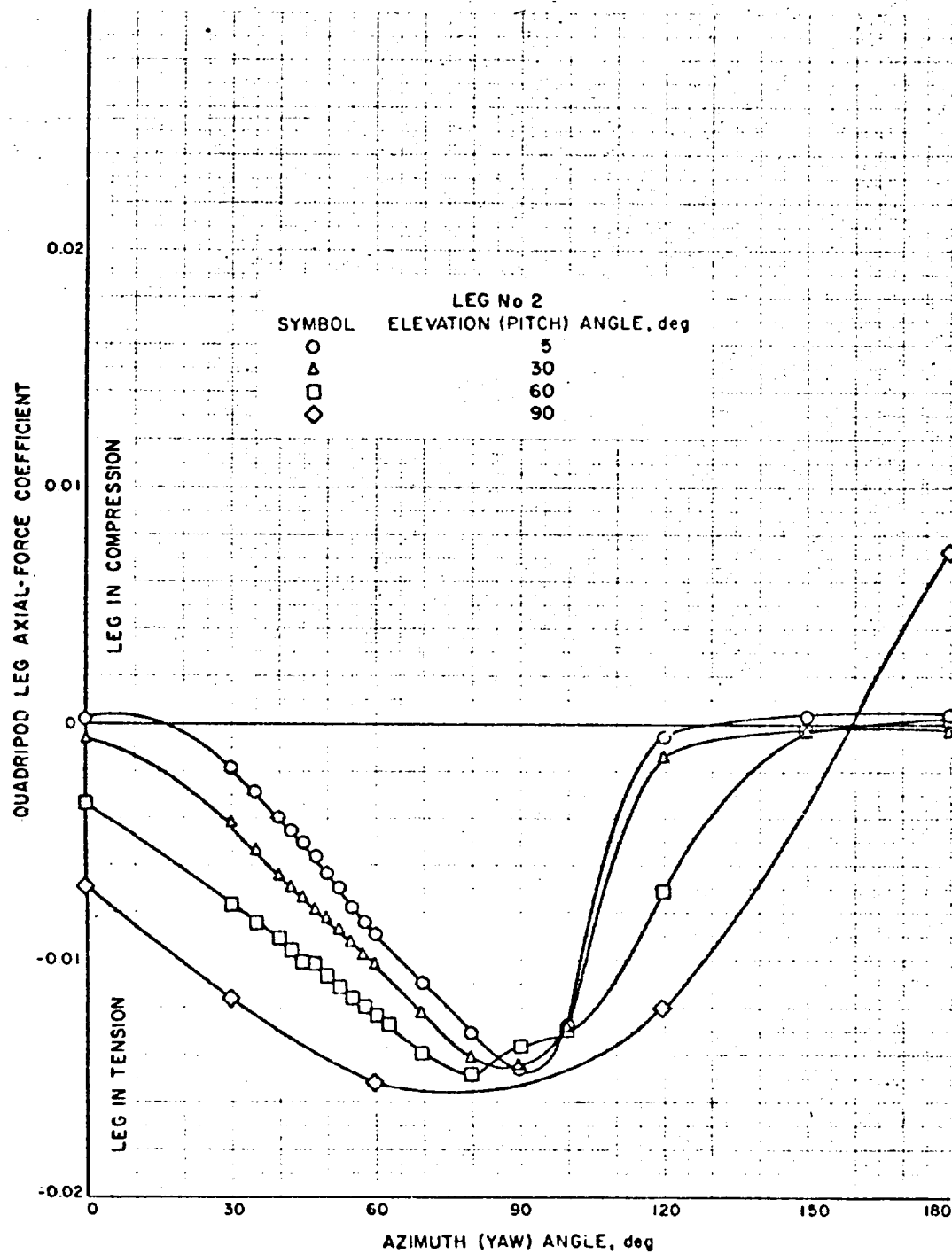


Fig. 42. Axial-force coefficient on leg 2 of quadripod structure

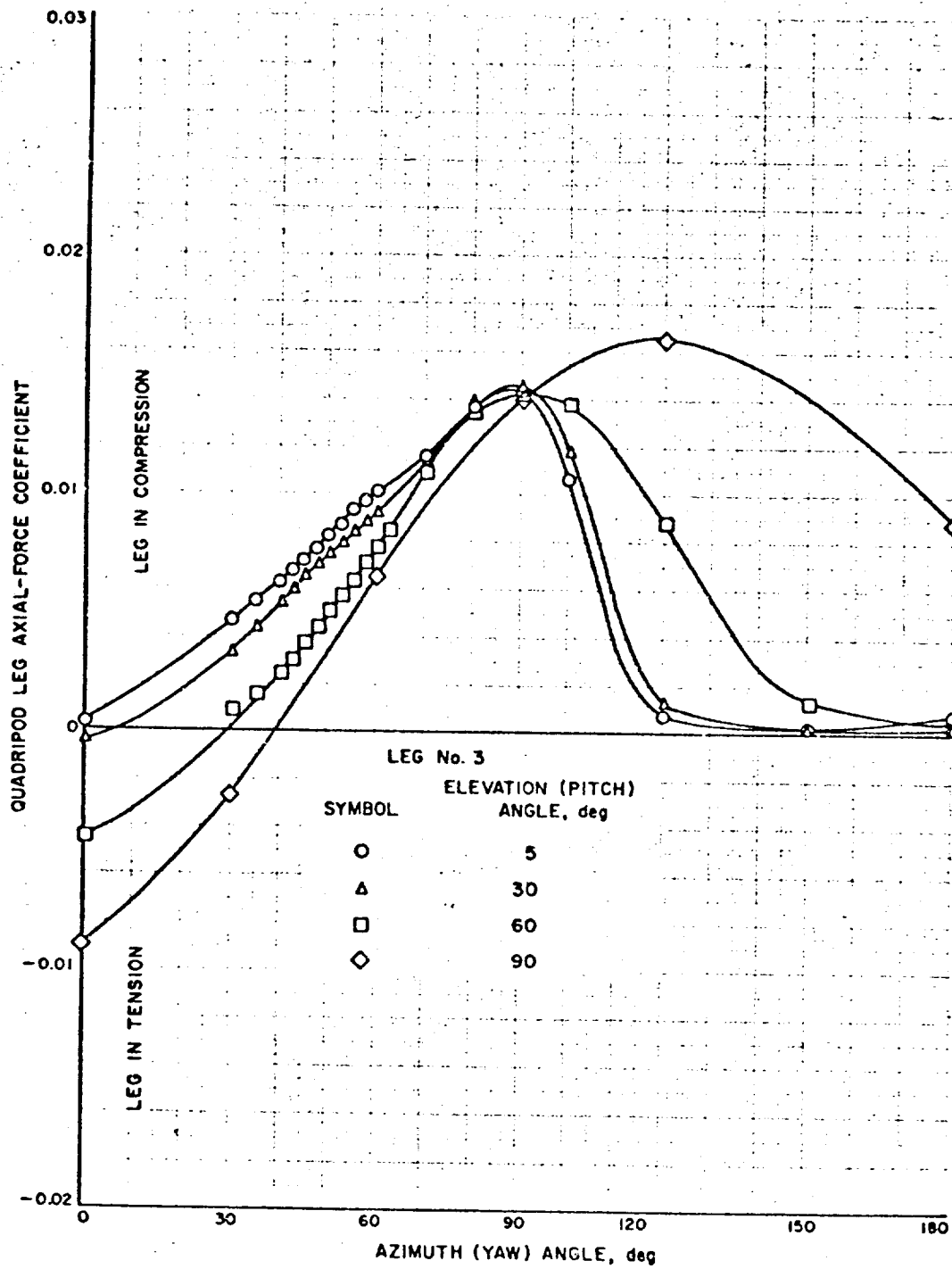


Fig. 43. Axial-force coefficient on leg 3 of quadripod structure

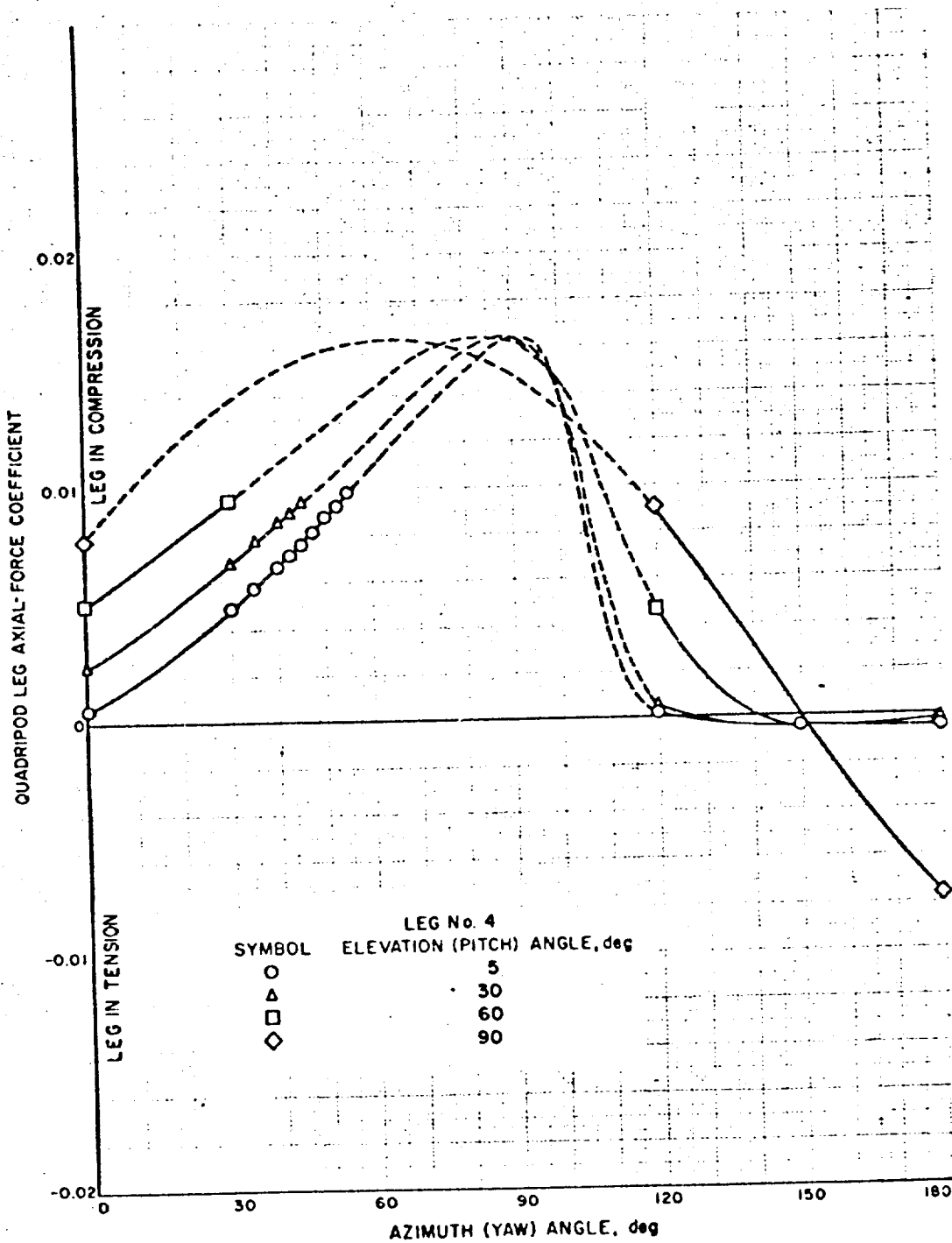


Fig. 44. Axial-force coefficient on leg 4 of quadripod structure